Title

Spatiotemporal Characterization of the Plasmin Activation System in a Rat Model of Acute Organophosphate Intoxication

Permalink

https://escholarship.org/uc/item/3sh5q2d5

Author

Blackmon, Thomas

Publication Date

2021

Supplemental Material

https://escholarship.org/uc/item/3sh5q2d5#supplemental

Peer reviewed|Thesis/dissertation

Spatiotemporal Characterization of the Plasmin Activation System in a Rat Model of Acute

Organophosphate Intoxication

By

THOMAS BLACKMON

THESIS

Submitted in partial satisfaction of the requirements for the degree of

MASTER OF SCIENCE

in

Pharmacology and Toxicology

in the

OFFICE OF GRADUATE STUDIES

of the

UNIVERSITY OF CALIFORNIA

DAVIS

Approved:

Pamela Lein, Chair

Fredric Gorin

Heike Wulff

Committee in Charge

2021

Abstract

Current therapeutic strategies for organophosphate (OP)-induced *status epilepticus* (SE) prevent mortality, but not chronic neurotoxic outcomes, which may be mediated in part by neuroinflammation. The plasminogen activation system (PAS) is implicated in diverse models of neuroinflammation but has yet to be evaluated after acute OP intoxication. Here, we characterized the PAS in a rat model of acute intoxication with diisopropylfluorophosphate (DFP). Adult male Sprague Dawley rats exposed to DFP (4 mg/kg, sc) followed 1 min later by atropine sulfate (2 mg/kg, im) and 2-pralidoxime (25 mg/kg, im) exhibited prolonged SE as determined using behavioral criteria. Electron microscopy of the hippocampus and piriform cortex at 1 day post-exposure (DPE) was consistent with metabolic stress and acute neurodegeneration. At 1 DPE, concentrations of plasminogen activator inhibitor-1 (PAI-1) were significantly increased in serum from DFP rats. Protein levels of the plasminogen activators (PA), tissue plasminogen activator (tPA) and urokinase plasminogen activator (uPA), as determined by ELISA, were elevated in the cerebellum, cortex and hippocampus in a time- and region-dependent manner after DFP exposure. Similarly, normalized protein levels of the primary PA inhibitor, PAI-1, was also elevated in the same brain regions. At 1 DPE, tPA, uPA and PAI-1 were significantly increased in the cortex and hippocampus. Normalized concentrations of uPA and PAI-1 returned to control values by 3-7 DPE, whereas tPA concentrations remained persistently elevated in the cortex and hippocampus up to 28 DPE. Immunohistochemistry confirmed increased PAI-1 immunoreactivity in multiple regions of the DFP brain up to 28 DPE. Co-localization of PAI-1 with neuronal, microglial and astrocytic biomarkers indicated that PAI-1 predominantly localized to astrocytic subsets, with intense immunofluorescence in astrocytic endfeet associated with endothelial cells. Collectively, these

data indicate that acute DFP intoxication activates the PAS, identifying this enzymatic cascade as a potential therapeutic target for mitigating the long-term neurologic consequences of acute OP intoxication.

1. **Introduction**

Organophosphorus (OP) compounds are used extensively around the world as pesticides, and some have been developed as potent nerve agents [23]. Many OPs cause neurotoxicity as a consequence of acetylcholinesterase (AChE) inhibition [23]. Acute inhibition of >60-80% of brain AChE activity can trigger convulsions that progress to life threating *status epilepticus* (SE) [4]. Survivors face significant long-term morbidity, including persistent neuropathology, mild-to-severe memory loss, and recurrent seizures [34, 52, 73]. It is posited that neuroinflammation contributes to the chronic neurotoxic effects of OP-induced SE [4, 42]. The neuroinflammatory response, which includes increased circulating levels of pro-inflammatory cytokines, such as TNF-alpha, TGF-beta, and IL-6, and the activation of astrocytes and microglia, can persist for months after exposure [41]. However, preclinical evaluation of therapeutic strategies that involve blocking neuroinflammatory responses have largely been unsuccessful in mitigating the long-term neurologic sequelae of acute OP intoxication [4].

The plasminogen activation system (PAS) includes the proteases, urokinase plasminogen activator (uPA) and tissue plasminogen activator (tPA), as well as endogenous protease inhibitors, such as plasminogen activator inhibitor-1 (PAI-1) (Fig. 1). While the primary physiologic role of this enzymatic cascade is regulation of the dissolution of blood clots, the PAS is also involved in angiogenesis, cell migration, wound healing, apoptosis, and the inflammatory response [2, 43]. As implied by their names, tPA and uPA activate plasminogen to plasmin, while PAI-1 binds uPA and tPA to effectively inhibit endogenous fibrinolysis and thrombolysis [49]. PAI-1 levels are increased in brain tissue after trauma and in age-related pathologies, and increased levels of PAI-1 are positively correlated with increased levels of proinflammatory cytokines, such as IL-1 alpha, IL-6, TNF-alpha, and TGF-beta [18, 22, 40, 70, 85]. PAI-1 is

expressed in activated astrocytes and has been used as a diagnostic marker in pathologies such as cancer and Alzheimer's disease [45, 47, 70, 81].

Recent publications have demonstrated the plausibility of PAI-1 inhibition as a therapeutic strategy for reducing inflammation in the periphery and in the brain. In neuroinflammatory models, such as experimental autoimmune encephalitis, uPA/tPA have been shown to be crucial in ameliorating the adverse neurologic effects of multiple sclerosis, and PAI-1 inhibition improves outcomes [43]. In a glioma model, inhibitors of PAI-1 that target an intracellular PAI-1/uPA complex caused endosomal mistrafficking and lysosomal degradation that induced apoptosis-inducing factor, resulting in caspase-independent necrosis [37, 38, 71]. These observations suggest that therapeutic strategies that trigger PAI-1-related endosomal mistrafficking may reduce neuroinflammation and increase activity of the PAS to promote recovery after trauma. In fact, many *in vitro* models have demonstrated the effectiveness of PAI-1 inhibition in increasing plasminogen activator function or killing proliferating cells [37, 38, 71]. Genetic deletion of PAI-1 further demonstrated that PAI-1 inhibition can reduce pathology in experimental mouse models of AD [63], MS [43], and lung injury [48].

The goal of this study is to characterize the spatiotemporal profile of PAS activation following acute OP intoxication as an initial step in evaluating the PAS as a potential therapeutic target for mitigating the chronic neurotoxic outcomes of OP-induced SE. For these studies, we used a rat model of acute intoxication with diisopropylfluorophosphate (DFP), which we and others have shown recapitulates both the acute and chronic neurologic sequelae observed in humans with OP poisoning [41, 75, 76].

2. __Methods and Materials__

2.1. Animals and Exposure

Animals were maintained in facilities fully accredited by the Association for Assessment and Accreditation of Laboratory Animal Care, and all studies were performed with regard to the alleviation of pain and suffering under protocols approved by the UC Davis Institutional Animal Care and Use Committee (IACUC protocol numbers 201865, 201954). Animal experiments were conducted in accordance with ARRIVE guidelines and the National Institutes of Health guide for the care and use of laboratory animals [24]. Adult male Sprague Dawley rats (250– 280 g; 6-8 weeks; Charles River Laboratories, Hollister, CA, USA) were housed individually in standard plastic cages under controlled environmental conditions (22 °C, 40–50% humidity) with a normal 12 h light/dark cycle. Food (Teklad Global 18% Protein Rodent Diet; Envigo, Livermore, CA, USA) and water were provided *ad libitum.* Table 1 illustrates the cohorts used throughout the study. To minimize the number of animals used, each animal was used for as many endpoints as feasible.

Animals were randomly assigned to experimental groups (DFP or vehicle (VEH)) using a random number generator function in Microsoft Excel. As illustrated in Figure 1, unanesthetized rats were administered DFP (90% +/- 7% pure as determined by [^{1}H]-NMR, Sigma Aldrich, St Louis, MO, USA) at 4 mg/kg, sc on the hindquarters, as described previously [84]. DFP was diluted in sterile ice-cold 0.2 M phosphate buffered saline (PBS; 3.6 mM Na_2HPO_4, 1.4 mM NaH_2PO_4, 150 mM NaCl, pH 7.2). VEH animals received the same volume (300 µL) of ice-cold PBS. DFP and VEH animals were administered atropine sulfate (purity 97%, Sigma Aldrich) at 2.0 mg/kg, im, and 2-pralidoxime (2-PAM, purity 97%, Sigma Aldrich) at 25 mg/kg in saline, im. These drugs significantly reduced mortality by blocking the peripheral parasympathomimetic

symptoms associated with acute OP intoxication [54]. The severity of seizure behavior was quantified using a 6-point scale as previously described [29, 84]. Seizure behavior was scored at 5 min intervals from 0 to 120 min post DFP injection and at 20 min intervals from 120 to 240 min post DFP injection. Seizure severity for each animal was quantified as the average seizure severity score, which is the average of the 16 scores collected during the initial 4 h post DFP. At 6 h post exposure, animals were injected, sc, with 10 ml of 5% w/v dextrose in saline (Baxter, Deerfield, IL, USA) and returned to their home cages. Rats were weighed daily post-exposure and provided moistened rat chow for 3–5 days until they were able to locate and consume standard chow and water independently. Subsets of animals from each experimental group were euthanized at 1, 3, 7, or 28 days post-exposure (DPE) via inhalation of 4% isoflurane in medical grade oxygen, and subsequent transcardial perfusion with cold PBS at a flow rate of 15 mL/min using a Masterflex peristaltic pump (Cole Parmer, Vernon Hills, IL, USA). Brains were removed and bisected sagittally, with one hemisphere dissected on ice to obtain the hippocampus, cortex and cerebellum, which were snap frozen in liquid nitrogen, and the other hemisphere processed for immunohistochemistry (IHC) (see section 2.5).

2.2. Electron Microscopy

A separate animal cohort was used to collect samples for EM because of the differences in sample preparation needed for EM imaging. Two Sprague Dawley rats were maintained under the same conditions and exposed to DFP or VEH as described in section 2.1. Their brains were collected for electron microscopy (EM) at 1 DPE. Samples were perfused as described in section 2.1. Coronal brain sections (2 mm thick) of the hippocampus and piriform cortex at -3.0 mm Bregma were post-fixed in 2.5% v/v glutaraldehyde (Ted Pella, Redding CA, USA), 2% w/v paraformaldehyde (PFA; Ted Pella) in 0.1 M PBS (26 mM NaH_2PO_4, 77 mM Na_2HPO_4, 400 mL

MilliQ H_2O, pH 7.3) provided by the Biological Electron Microscopy Facility Core at the University of California, Davis. After fixation for 96 h at 4 °C, tissues were rinsed twice in 0.1 M PBS for a total of 30 min and then placed in 1% w/v osmium tetroxide (Electron Microscopy Sciences, Hatfield, PA, USA) in 0.1 M PBS for 1 h. Tissues were rinsed twice for 15 min each in 0.1 M PBS. The samples were next dehydrated in a series of graded ethanol (50%, 75%, 95% for at least 30 min each and 100% twice for 20 min). Tissues were washed twice in propylene oxide (Electron Microscopy Sciences) for 15 min and then pre-infiltrated in half resin (composed of 450 mL dodecenyl succinic anhydride, 250 mL araldite 6005, 82.5 mL Epon 812, 12.5 mL dibutyl phthalate, and 450 uL benzyl dimethylamine; Electron Microscopy Sciences) and half propylene oxide overnight. The following day, tissues were infiltrated in 100% resin for 5 h. The tissues were embedded with fresh resin and polymerized at 60 °C overnight. The embedded tissues were sectioned using a Leica EM UC6 ultramicrotome (Leica Biosystems Inc., Buffalo Grove, IL, USA) at a thickness of 90 nm and collected on copper mesh grids. Sections were stained with 4% w/v aqueous uranyl acetate (Ted Pella) for 20 min and for 2 min in 0.2% w/v lead citrate (Eastman, Kingsport, TN, USA) in 0.1 N NaOH. Representative images of all time points and treatments were acquired at the Biological Electron Microscopy Facility Core at the University of California, Davis using the FEI Talos L120C transmission electron microscope at 80kv and Thermo Scientific Ceta 16MP camera (Thermo Scientific, Waltham, MA, USA).

2.3. Plasmin Activity Assay

Total plasma plasmin activity was measured using the Sensolyte AFC Plasmin Activity Assay kit (Anaspec, Fremont, CA, USA; RRID:SCR_002114) following the manufacturer's instructions. Plasma samples were transferred to a 96 well microplate undiluted and incubated for 1 h at room temperature in darkness. Excess plasmin substrate permitted active plasmin

enzymatic concentration to be determined using the end point analysis provided by the manufacturer. Plasmin activity was assessed using a Synergy H1 microplate reader (λ_{Ex}=380 nm, λ_{Em}=500 nm; BioTek, Winooski VT, USA).

2.4. ELISA

Total PAI-1 plasma levels were measured using the RPAIKT-TOT ELISA kit (Molecular Innovations, Novi, MI, USA), following the manufacturer's instructions. Total PAI-1 measured by this ELISA included free PAI-1 and PAI-1 complexed to either tPA or uPA. Total plasma protein levels were measured with the Pierce BCA Protein Assay Kit (Thermo Scientific, Waltham, MA, USA), following the manufacturer's instructions for microplate assays. The total PAI-1 level in each sample was normalized to the plasma protein concentration in the same sample. Samples were diluted 1:40 to 1:80 with the same buffer used for the ELISAs but without the addition of bovine serum albumin (BSA).

Total PAI-1, tPA, and uPA levels in brain homogenates were measured using the RPAIKT-TOT, RTPAKT-TOT, and RUPAKT-TOT ELISA kits (Molecular Innovations), respectively, following the manufacturer's instructions. To prepare brain homogenates, frozen brain tissue was weighed, and 0.1 M Tris-HCl buffer (TBS; 96 mM Tris-HCl, 187 mM NaCl, 50 mL MQ H_2O, pH 8.5) with 0.1% w/v Triton X-100 (Thermo Fisher), was added at 1 mL per 0.1 g tissue. Large samples, like the cortex (COR), were crushed with a spatula in a 15 mL blood tube with TBS + Triton X-100 buffer on ice and then sonicated. Smaller samples, like the hippocampus (HC) and cerebellum (CER), were placed in 5 mL blood tubes or 1 mL centrifuge tubes based on the volume needed for sonication. Tissue was sonicated using a Virtis ultrasonic probe sonicator at power level 3 with 2-3 s bursts until > 95% of the tissue was homogenized. Sonicated tissue was aliquoted into 1 mL volumes and centrifuged at 21,000 X g for 30 min at 4 °C using an

Eppendorf 5417R centrifuge (Eppendorf, Enfield, CT, USA). Supernatant was removed, transferred to the ELISA microplate wells, and diluted 1:10 in blocking buffer (3% w/v BSA in TBS; 96 mM Tris-HCl, 187 mM NaCl, 40 mL MQ H_2O, pH 7.4, then add 10 mL MQ H_2O). Total brain supernatant protein levels were quantified using the Pierce BCA Protein Assay Kit (Thermo Scientific), following the manufacturer's instructions for microplate assays. Samples were diluted 1:10 in the same buffer used for ELISAs but without the addition of BSA. Total PAI-1 concentration in each sample were normalized to total protein concentration in the same sample. ELISA and BCA assays were read using a Synergy H1 microplate reader at 450 nm and 562 nm, respectively (BioTek).

2.5. Immunohistochemistry (IHC)

Brain tissue used for IHC was blocked on ice in 2-mm thick coronal sections immediately after harvest from the skull and post-fixed in 4% w/v PFA (Sigma Aldrich) for 24 h at 4 °C. Tissue blocks were transferred to 30% w/v sucrose (Sigma Aldrich) in PBS and stored at 4 °C for at least 48 h until embedded and flash frozen in Tissue-Plus™ O.C.T. compound (Thermo Fisher Scientific). Tissue blocks were cryosectioned into 10 μm thick coronal sections and stored at −80 °C until immunostained. Slides were immunostained in batches, including a negative control slide (see Figures S7-S10 in Supplemental) that was incubated with blocking buffer containing no primary antibody but otherwise processed identically to sections stained with primary antibody. Slides were removed from -80 °C storage, brought to room temperature, dried, and then washed with PBS for 5 min before antigen retrieval. Antigen retrieval consisted of submerging slides in 10 mM sodium citrate buffer (Thermo Fisher), pH 6.0, and heating in a rice cooker for 40-45 min at 60°-70°C, refilling buffer as needed. After antigen retrieval, tissue sections were washed twice in PBS + 0.03% w/v Triton X-100 (PBS-T), circled with a

hydrophobic PAP-Pen marker, and incubated for 1 h at room temperature in blocking buffer of either 10% v/v normal goat serum (Vector Laboratories, Burlingame, CA, USA) + 1% w/v BSA (Sigma Aldrich) in 0.03% PBS-T or 5% v/v donkey serum (Millipore Sigma, Burlington, MA, USA) in 0.03% PBS-T, depending on the species of the primary antibody. Sections were incubated with primary antibody (Table 2) in blocking buffer at 4°C overnight in the dark. The following day, sections were washed four times for 5 min in PBS-T. Sections were recircled with a hydrophobic marker and incubated in secondary antibodies (Table 3) diluted in blocking buffer for 1 h at room temperature in the dark. Sections were then washed twice for 5 min with PBS. Slides were cover slipped in Prolong Gold with DAPI mounting media (Invitrogen, Carlsbad CA, USA) and cured overnight at room temperature before imaging. PAI-1 antibody was validated by western blotting (see Supplemental Methods 7.1; see Supplemental Figures S5, S6) and antibodies specific for NeuN [65], GFAP [31], IBA1 [3], CD68 [30], and CD31 [88] have been previously validated.

2.6. Image Acquisition and Analysis

Fluorescent images were acquired using the ImageXpress Micro XLS High Content Analysis System (Molecular Devices, Sunnyvale, CA, USA). Positive immunostaining was identified as signal that was at least twice background intensity in the same sample. Using a photographic rat brain atlas [57] to confirm anatomical structures, images of the following brain regions were acquired from Bregma -2.5mm to -4.5mm: 1) dentate gyrus (DG) of the hippocampus, 2) thalamus, 3) piriform cortex, 4) CA1 region of the hippocampus, 5) CA3 region of the hippocampus, and 6) amygdala. Multiple overlapping tiles were stitched together to produce an image containing the entire brain region that was then used for image analysis using MetaXpress High-Content Imaging Analysis and Software version 6.1. Outcomes analyzed

included count of cells immunopositive for PAI and colocalization of PAI-1 immunoreactivity with a biomarker of specific cell types. Immunoreactivity was assessed with respect to the percentage of cells in the field of view (identified by DAPI staining) that were immunopositive for the biomarker of interest using the Multi Wavelength Cell Sorting Journal within the Custom Module Editor image analysis software (MetaXpress High-Content Image Acquisition and Analysis software, version 6.1, Molecular Devices). The custom modules used for these analyses can be found in Supplemental Methods 7.2. Representative images of all experimental groups were acquired from the same slides used for quantification using a Leica SP8 STED microscope equipped with a 63x objective available through the Advanced Imaging Facility Core at the University of California, Davis. These images were edited using FIJI software version 2.1.0/1.53c.

2.7. Statistics

2.7.1 Plasmin Activity Assay

Mixed effect models, including animal-specific random effects, were used to assess differences between DFP and VEH groups and time post-exposure (1, 3, 7, or 28 days post-exposure). Concentrations of active plasmin were transformed using the natural logarithm to meet the assumption of normality for the mixed effect models. Akaike Information Criterion (AIC) was used to find the best model for each outcome [17]. To assess group differences (DFP vs VEH) by time, Benjamini-Hochberg False Discovery Rate (FDR) was used to determine comparisons that remained significant after accounting for multiple testing. All results are presented as the geometric ratio between DFP and VEH. R (version 3.6.0, R Core Team (2019), Vienna, Austria) was used for all analyses and to output graphics.

2.7.2 ELISA

Mixed effect models, including animal-specific random effects, were used to assess differences between DFP and VEH groups by brain region (CER, COR, HC) and time post-exposure (1, 3, 7, or 28 days post-exposure). All outcomes of interests (PAI-1, tPA, and uPA) were transformed using the natural logarithm to meet the assumption of normality for the mixed effect models. Akaike Information Criterion (AIC) was used to find the best model for each outcome. To assess group differences (DFP vs VEH) by region or/and time (depends on the best model), Benjamini-Hochberg False Discovery Rate (FDR) was used to determine comparisons that remained significant after accounting for multiple testing [12]. All results are presented as the geometric ratio between DFP and VEH. SAS (version 9.4, SAS Institute, Inc., Cary, NC, USA) was used for all analyses, and R (version 3.6.0, R Core Team (2019), Vienna, Austria) was used to output graphics. Sample sizes were determined *a priori* using a power analysis software (G*Power version 3.1) [33]. The two-tailed t-test of the differences between two independent means used an effect size of 2, and alpha of 0.05, a power level of 0.8, and an allocation ratio of 2.

2.7.3 Quantitative IHC

The primary outcomes were colocalization of PAI-1 and GFAP, PAI-1 and IBA1, PAI-1 and CD68, and PAI-1 and NeuN. Mixed effects models, including animal-specific random effects, were fit to assess differences between exposure groups. Primary factors of interest included exposure (DFP, VEH), region (amygdala, CA1, CA3, dentate gyrus, piriform cortex, thalamus), and time post exposure (1, 3, 7, 28 days post-exposure). Interactions between the factors (exposure, region, and time point) were considered and the best model was chosen using AIC. The outcome was transformed using the natural logarithm after shifting all values by a small number (0.1 for PAI-1/IBA-1 and PAI-1/CD68 colocalization, 0.5 for PAI-1/NeuN, and 1

for PAI-1/GFAP colocalization) to enable the calculation for the animals with no colocalization to better meet the assumptions of the model. Contrasts for group differences were constructed and tested using a Wald test. The FDR was used to account for multiple comparisons across contrasts. Results are presented as geometric mean ratios (GMR) between exposure groups. Point estimates of the ratios and 95% confidence intervals are presented in the figures. When the confidence interval for the GMR includes 1, there is no statistical evidence of a difference between groups. All analyses were performed using SAS software, version 9.4 and alpha was set at 0.05; results remained significant after implementation of the FDR procedure unless otherwise stated.

3. Results

3.1 Acute brain injury associated with DFP-induced *status epilepticus*

Animals acutely intoxicated with DFP exhibited seizure behavior within minutes after exposure to DFP that lasted for hours (Fig. 2c), as indicated by an average seizure score ≥ 2.5 across the first 4 h after injection of DFP. Previous studies have confirmed that seizure scores of 3 or higher corresponded to *status epilepticus* and induced robust neuroinflammatory responses [29, 76, 84]. Electron microscopy of brain sections from animals 1 DPE (Fig. 3) revealed evidence of early neuronal degeneration in both the piriform cortex and hippocampus of the DFP animal. Injured neurons demonstrated abnormal distribution of elongated rough endoplasmic reticulum lacking Nissl formation, ribosomal detachment indicating early chromatolysis, and mitochondrial swelling with distorted cristae. Dark neurons and microglia are consistent with oxidative injury and the abnormal mitochondrial localization and appearance was restricted to the DFP animal. Dilation of the neuronal endoplasmic reticulum (ER) is also consistent with

acute, generalized neuronal dysfunction compounded by oxidative stress [19]. Samples from the DFP animal had large numbers of free polyribosomes with enlarged mitochondria containing an increased electron-dense matrix that are often present within the neuronal soma rather than being restricted within the dendritic or axonal processes. Samples from the VEH animal appeared normal and were without the corresponding mitochondrial abnormalities or vacuolation, confirming early signs of pathology restricted to the DFP animal.

3.2. Acute DFP intoxication activates the peripheral plasminogen activation system

Previous studies of plasmin knockout mice and cerebral ischemia models have confirmed that neuroinflammation and changes within the PAS are linked [7, 74], raising the question of whether this association extends to acute OP intoxication. To determine whether acute DFP intoxication affects the balance of the PAS, we first measured blood plasmin concentration in the plasma from VEH and DFP animals at 1, 3, 7, 28 days post-exposure. Mean plasma plasmin concentrations were not significantly different across any time points but were elevated at 1 DPE (Fig. 4a-b; VEH 1.56 μM active plasmin; DFP 1.15 μM active plasmin; GMR=2.09, 95% CI: (0.3, 13.1), p=0.419) and 3 DPE (Fig. 4a-b; VEH 0.689 μM active plasmin; DFP 1.17 μM active plasmin; GMR=1.78, 95% CI: (0.2, 16.6), p=0.600). This observation indicates an induction of pro-inflammatory conditions in DFP-intoxicated animals [6, 27]. DFP animal plasma plasmin concentrations at 7 DPE (Fig. 4a-b; VEH 0.637 μM active plasmin; DFP 0.486 μM active plasmin; GMR=0.2, 95% CI: (0.02, 1.6), p<0.128) and 28 DPE (Fig. 4a-b; VEH 0.410 μM active plasmin; DFP 0.535 μM active plasmin; GMR=1.41, 95% CI: (0.2, 8.9), p<0.702) returned and remained at baseline.

Even though there was not a general increase in active plasmin concentrations, we wanted to confirm the components within the PAS changed, so we next determined whether this

reflected DFP effects on specific molecular components of the PAS. Quantification of plasma

PAI-1 levels in DFP versus VEH animals by ELISA indicated a tenfold increase in PAI-1 plasma

concentrations at 1 DPE (Fig. 5a-b; VEH 0.016 PAI-1/mg protein; DFP 0.149 ng PAI-1/mg

protein; GMR=6.83, 95% CI: (3.0, 15.4), p<0.001). DFP animals had two-fold higher

concentrations of PAI-1 at 3 DPE (Fig. 5a-b; VEH 0.014 PAI-1/mg protein; DFP 0.026 ng PAI-

1/mg protein; GMR=1.7; 95% CI: (0.8, 3.6); p=0.172). PAI-1 concentrations in DFP animals

returned to baseline at 7 DPE (Fig. 5a-b; VEH 0.015 PAI-1/mg protein; DFP 0.024 ng PAI-1/mg

protein; GMR=1.2; 95% CI: (0.5, 2.7); p=0.640) and 28 DPE (Fig. 5a-b; VEH 0.021 PAI-1/mg

protein; DFP 0.022 ng PAI-1/mg protein; GMR=0.7; 95% CI: (0.3, 1.6); p=0.406).

3.3 Acute DFP intoxication alters components of the PAS in the brain

Peripheral activation of the PAS could influence PAS components within the brain, so we

next measured levels of tPA, uPA, and PAI-1 in three brain regions: cerebellum, cortex, and

hippocampus [8]. Cerebellar tPA concentrations were relatively stable in both VEH and DPF

animals at all time points. There was no statistical difference found between DFP and VEH

cerebellar tPA concentrations at 1, 3, 7, and 28 DPE (Fig. 6a-b; VEH 3.74, 3.32, 3.72, and 3.41

ng tPA/mg protein; DFP 3.01, 3.43, 3.26, and 3.19 ng tPA/mg protein respectively; GMR=0.9;

95% CI:(0.8, 1.0); p=0.179). Cortical tPA concentrations were increased approximately two-fold

in DFP animals compared to VEH at 1, 3, and 7 DPE but returned to control levels by 28 DPE.

In the cortex, there were no statistically significant differences when comparing each time point

but there was an overall significant difference between DFP and VEH animals (Fig. 6a-b; VEH

1.80, 1.92, 1.89, 2.14 ng tPA/mg protein; DFP 2.15, 2.49, 2.15, and 1.91 ng tPA/mg protein;

GMR=1.4; 95% CI: (1.2, 1.6) p<0.001). In the hippocampus, tPA concentrations were increased

two to three-fold in DFP animals compared to VEH animals at all time points. There was no

significant difference in hippocampal tPA concentrations across time points, so estimates of group differences were averaged across time points (Fig. 6a-b; VEH 0.79, 0.91, 1.02, and 1.01 ng tPA/mg protein; DFP 2.15, 2.49, 2.15, and 1.91 ng tPA/mg protein; GMR=2.2; 95% CI:(1.9, 2.6); p<0.001).

Another key serine protease in the PAS is uPA, which influences CNS functions such as cellular adhesion and migration and has been implicated in other models of neuroinflammation [25, 62]. Concentrations of uPA in the cerebellum were significantly decreased in DFP animals at 1 DPE (Fig. 6c-d; VEH 0.15 uPA/mg protein; DFP 0.11 ng uPA/mg protein; GMR=0.7; 95% CI: (0.5, 0.9); p=0.005). Cerebellar uPA concentrations in DFP animals returned to baseline at 3 DPE (Fig. 6c-d; VEH 0.11 ng uPA/mg protein; DFP 0.12 ng uPA/mg protein; GMR=1.1; 95% CI: (0.8, 1.6); p=0.500) and remained at baseline levels at 7 DPE (Fig. 6c-d; VEH 0.13 ng uPA/mg protein; DFP 0.16 ng uPA/mg protein GMR=1.2; 95% CI: (0.9, 1.5); p=0.277) and 28 DPE (Fig. 6c-d; VEH 0.12 ng uPA/mg protein; DFP 0.13 ng uPA/mg protein GMR=1.0; 95% CI: (0.6, 1.7); p=0.901). Concentrations of uPA in the cortex were increased four-fold in DFP animals compared to VEH at 1 DPE (Fig. 6c-d; VEH 0.09 ng uPA/mg protein; DFP 0.35 ng uPA/mg protein; GMR=4.1, 95% CI: (2.8, 6.2), p<0.001). At 3 DPE, uPA concentrations in DFP animals were about twofold higher than VEH animals; however, this difference was not statistically significant (Fig. 6c-d; VEH 0.18 ng uPA/mg protein; DFP 0.30 ng uPA/mg protein; GMR=1.8; 95% CI: (0.8, 3.8); p=0.139). Cortical uPA concentrations at 7 DPE (Fig. 6c-d; VEH 0.18 ng uPA/mg protein; DFP 0.24 ng uPA/mg protein; GMR=1.2; 95% CI: (0.8, 1.9); p=0.458) and 28 DPE (Fig. 6c-d; VEH 0.10 ng uPA/mg protein; DFP 0.16 ng uPA/mg protein; GMR=1.6; 95% CI: (0.9, 2.9); p=0.140) were not significantly increased compared to time-matched VEH animals. Hippocampal uPA concentrations were increased fivefold in DFP animals compared to

VEH animals at 1 DPE (Fig. 6c-d; VEH 0.09 ng uPA/mg protein; DFP 0.49 ng uPA/mg protein; GMR=5.3, 95%CI: (4.1, 6.8), p<0.001). Hippocampal uPA concentrations in DFP animals were two to three-fold higher at 3 DPE (Fig. 6c-d; VEH 0.07 ng uPA/mg protein; DFP 0.25 ng uPA/mg protein; GMR=3.5; 95% CI: (1.5, 8.0); p=0.004) and 7 DPE (Fig. 6c-d; VEH 0.09 ng uPA/mg protein; DFP 0.21 ng uPA/mg protein; GMR=2.0; 95% CI: (1.3, 3.2); p=0.002). At 28 DPE, hippocampal uPA concentrations were not significantly elevated compared to time-matched VEH animals (Fig. 6c-d; VEH 0.09 ng uPA/mg protein; DFP 0.19 ng uPA/mg protein; GMR=1.9; 95% CI: (0.7, 5.1); p=0.231).

One of the key inhibitors of tPA and uPA is PAI-1, so we next measured levels of PAI-1 to determine if PAI-1 expression differed in the brain compared to plasma. PAI-1 concentrations in the cerebellum were significantly increased threefold at 1 DPE (Fig. 6e-f; VEH 0.10 PAI-1/mg protein; DFP 0.28 ng PAI-1/mg protein; GMR=3.1, 95% CI: (1.4, 6.6), p=0.004). Cerebellar PAI-1 concentrations in DFP animals remained elevated at 3 DPE (Fig. 6e-f; VEH 0.13 ng PAI-1/mg protein; DFP 0.36 ng PAI-1/mg protein GMR=2.5; 95% CI: (1.0, 6.0); p=0.045) but returned to baseline concentrations at 7 DPE (Fig. 6e-f; VEH 0.30 ng uPA/mg protein; DFP 0.18 ng uPA/mg protein GMR=0.9; 95% CI: (0.3, 2.2); p=0.788) and 28 DPE (Fig. 6e-f; VEH 0.13 ng uPA/mg protein; DFP 0.17 ng uPA/mg protein GMR=1.3; 95% CI: (0.6, 2.7); p=0.490). PAI-1 concentrations in the cortex were increased approximately forty-fold in DFP animals compared to VEH at 1 DPE (Fig. 6e-f; VEH 0.08 ng PAI-1/mg protein; DFP 2.99 ng PAI-1/mg protein; (GMR=37.3, 95% CI: (22.0, 63.4), p<0.001). At 3 DPE, cortical PAI-1 concentrations in DFP animals were about six-fold higher than VEH animals (Fig. 6e-f; VEH 0.12 ng PAI-1/mg protein; DFP 0.78 ng PAI-1/mg protein; GMR=5.4, 95% CI: (2.4, 12.4), p<0.001). Cortical PAI-1 concentrations at 7 DPE were not significantly elevated (Fig. 6e-f; VEH 0.10 ng PAI-1/mg

protein; DFP 0.60 ng PAI-1/mg protein; GMR=2.3; 95% CI: (0.8, 7.0); p=0.141). DFP cortical

PAI-1 concentrations at 28 DPE were slightly decreased compared to VEH animal but were not

significantly different (Fig. 6e-f; VEH 0.13 ng PAI-1/mg protein; DFP 0.07 ng PAI-1/mg

protein; GMR=0.5; 95% CI: (0.3, 1.0); p=0.036). PAI-1 concentrations in the hippocampus were

increased thirty-fold in DFP animals compared to VEH animals at 1 DPE (Fig. 6e-f; VEH 0.08

ng PAI-1/mg protein; DFP 2.49 ng PAI-1/mg protein; GMR=27.7, 95% CI: (20.8, 37.0),

p<0.001). Hippocampal PAI-1 concentrations in DFP animals were six-fold higher than VEH at

3 DPE (Fig. 6e-f; VEH 0.12 ng PAI-1/mg protein; DFP 0.75 ng PAI-1/mg protein; GMR=4.4,

95% CI: (2.2, 8.7), p<0.001). Hippocampal PAI-1 concentrations in DFP dropped to slightly

above VEH levels at 7 DPE (Fig. 6e-f; VEH 0.18 ng PAI-1/mg protein; DFP 0.26 ng PAI-1/mg

protein; GMR=1.7; 95% CI: (0.8, 3.7); p=0.170). At 28 DPE, hippocampal PAI-1 concentrations

returned to VEH baseline levels (Fig. 6e-f; VEH 0.11 ng PAI-1/mg protein; DFP 0.17 ng PAI-

1/mg protein; GMR=1.3; 95% CI: (0.8, 2.2); p=0.214).

3.4. Regional and cellular distribution of PAI-1 in the brain after acute DFP intoxication

ELISA and plasmin activity assays demonstrated that acute DFP intoxication caused

significant changes in the PAS in the brain, therefore, we next characterized the expression of

PAI-1 using IHC to determine whether PAI-1 expression was relegated to specific regions within

the brain. PAI-1 immunoreactivity was examined at 1, 3, 7, and 28 DPE in the dentate gyrus,

CA1 and CA3 subregions of the hippocampus, thalamus, amygdala, and piriform cortex of VEH

and DFP animals. These brain regions were chosen because they exhibit significant

neurodegeneration, microgliosis and reactive astrogliosis following acute DFP intoxication [41,

84]. At 1 and 3 DPE, weak PAI-1 positive immunoreactivity was found in the dentate gyrus and

CA1 subregions of the hippocampus, the thalamus, and the amygdala, but no positive PAI-1

staining was observed in the CA3 subregion of the hippocampus or piriform cortex (see Figure S1, S2 in Supplemental materials). At 7 DPE, PAI-1 immunoreactivity was found in in all brain regions examined except the thalamus, which only occasionally presented positive immunoreactivity, primarily around blood vessels (see Figure S3, S4 in Supplemental materials). At 28 DPE, strong PAI-1 immunostaining was found in the hilus of the dentate gyrus (Fig. 7a-b), concentrated towards the tip, the CA1 (Fig. 7c-d), CA3 (Fig. 7e-f), and the amygdala (Fig. 7g-h). Positive PAI-1 immunostaining was also observed in the thalamus (Fig. 7i-j), and piriform cortex (Fig. 7k-l), but not to the same degree as the other brain regions.

We next determined if PAI-1 was expressed by specific cell types in the brain. Initially, brain sections were co-labeled for PAI- and NeuN, a biomarker of mature neurons [65]. Representative photomicrographs of PAI-1/NeuN positive immunoreactivity in VEH and DFP brain tissue illustrate that PAI-1 positive immunoreactivity increases overall after DFP exposure but is not co-localized to NeuN immunoreactivity at any time point (Fig. 8). However, strong PAI-1 immunoreactivity appears adjacent to neurons. Quantitative analyses demonstrate that DFP did not induce PAI-1 expression in neurons in the DG of the hippocampus, CA1 of the hippocampus, CA3 of the hippocampus, or thalamus. However, significantly elevated colocalization of PAI-1 and NeuN in DFP animals relative to VEH animals was observed in the amygdala (GMR=3.4, 95% CI=1.6-7.4, p=.002) and piriform cortex (GMR=4.3, 95% CI=1.5-12.5, p=.007) (Fig. 8b). The piriform cortex and amygdala exhibit increased overall PAI-1 expression, similar to representative photomicrographs of the DG of the hippocampus, especially at 28 DPE when PAI-1 immunostaining overlaps NeuN immunoreactivity in both regions. There was no significant difference in the PAI-1/NeuN exposure effect by time point, so estimates of group differences were averaged across time points.

The data from PAI-1/NeuN colocalization suggested that another cell type, possibly glial cells adjacent to neurons may be expressing PAI-1. Therefore, we next determined whether PAI-1 expression co-localized with immunoreactivity for IBA1, a biomarker for microglial cells [3], which are known to become activated after DFP intoxication [35, 41]. To identify phagocytic microglia, we co-labeled sections for PAI-1 and CD68 [30]. Representative photomicrographs of PAI-1/IBA1/CD68 positive immunoreactivity in VEH and DFP brain slices illustrate that PAI-1 immunoreactivity increased overall after DFP exposure (Fig. 9). Importantly, strong PAI-1 immunoreactivity appeared in the PAI-1/IBA1/CD68 co-stain at 28 DPE, consistent with PAI-1/NeuN photomicrographs. Although quantitative analyses using high content imaging indicated that PAI-1 overlapped with IBA1 immunoreactivity in all regions of the DFP brain at all time points compared to VEH animals, confocal photomicrographs showed that positive co-staining reflected proximity of microglial processes to processes and/or cell bodies of another cell type (Fig.9; GMR=1.9, 95% CI:(1.0, 3.6), p=(.047)). This is not direct colocalization since neither cell bodies nor processes of microglia were immunoreactive for PAI-1 in their entirety. Quantitative analysis of PAI-1/CD68 co-staining demonstrated no significant differences between DFP and VEH animals in the DG of the hippocampus, CA1 of the hippocampus, CA3 of the hippocampus, or the thalamus. The only regions with significant differences in PAI-1/CD68 co-staining in DFP vs. VEH brains were the amygdala (Fig.9a, GMR=3.5, 95% CI=1.4-8.6, p=.007) and piriform cortex (GMR=2.9, 95% CI=1.1-8.2, p=.04), although only the amygdala remained significant after FDR (Fig. 9). There was no significant difference in the PAI-1/CD68 exposure effect by time point, so estimates of group differences were averaged across time points.

Astrocytes were shown to express PAI-1 in other models of inflammation [36, 50], so we next determined whether astrocytes express PAI-1 in the DFP brain. To identify astrocytes, we co-labeled brain sections for PAI-1 and GFAP, a marker of reactive astrocytes [31]. Representative photomicrographs of PAI-1 and GFAP immunoreactivity illustrate that PAI-1 immunoreactivity increased in all brain regions after DFP exposure (Fig. 10). Strong PAI-1 immunoreactivity was evident at 28 DPE (Fig. 8, 9). In DFP animals, PAI-1 immunostaining was observed in astrocyte cell bodies and processes (arrows; Fig. 10). There was no significant difference in the PAI-1/GFAP exposure effect by region, so estimates of group differences were averaged across regions. The percentage of astrocytes expressing PAI-1 was higher in DFP animals (n=10-12) compared to time-matched VEH animals (n=10-12) at 1 DPE (GMR=2.1, 95% CI: (1.5-3.0), p<.001), 7 DPE (GMR=3.0, 95% CI: (1.3-6.9), p=.010), and 28 DPE (GMR=7.0, 95% CI: (3.6-13.6), p<.001). The percentage of astrocytes expressing PAI-1 was not significantly increased in DFP animals compared to VEH animals at 3 DPE (GMR=0.7, 95% CI: (0.5-1.1), p=.200; Fig. 10a).

Images of PAI-1 and GFAP co-labeled brain sections suggested that PAI-1 might be expressed in astrocytic endfeet lining blood vessels in the brain. To assess this possibility, we co-labeled brain sections for CD31, a marker of endothelial cells [88], and PAI-1. Representative photomicrographs of PAI-1/CD31 immunoreactivity demonstrate general colocalization of PAI-1 near endothelial cells after acute OP intoxication (Fig. 11a-b). At higher magnification, there is colocalization of endothelial cells with PAI-1, however, it is reduced, and PAI-1 appears to primarily stain glial cell bodies and processes surrounding the endothelial cells (Fig. 11c). Both astrocytes and endothelial cells are known to express PAI-1, so it is likely that both cells are concurrently expressing PAI-1 at 1 DPE.

4. <u>Discussion</u>

Characterization of components of the PAS following DFP-induced SE indicates that the PAS is activated in a rat model of acute organophosphate intoxication. We found that plasma PAI-1 levels were acutely elevated after acute DFP intoxication although there was marked variance within DFP-exposed animals. This variation in active plasmin is associated with markedly elevated but variable levels of PAI-1, which is the primary peripheral inhibitor of the plasmin activators, uPA and tPA. As early as 1 DPE, ELISA analyses documented increased protein levels of tPA, uPA, and PAI-1 levels in the cortex and hippocampus of DFP-exposed animals relative to VEH controls. Levels of tPA remained persistently elevated throughout the 28 day period following DFP exposure, while uPA and PAI-1 levels returned to control values between 7 and 28 DPE. In contrast, there were only transient changes in PAS protein levels in the DFP cerebellum, with uPA levels significantly decreased at 1 DPE, and PAI-1 significantly increased at 1 DPE before returning to control levels by 3 DPE. Immunohistochemical characterization demonstrated PAI-1 immunoreactivity in astrocytes that become progressively more intense and widespread such that by 28 DPE, there was very bright PAI-1 immunofluorescence evident in the dentate gyrus, CA1 and CA3 regions of the hippocampus, piriform cortex, thalamus, and amygdala. These same brain regions have previously been shown to exhibit persistent neurodegeneration, neuroinflammation, and progressive gliosis in this rat model of acute DFP intoxication [4]. The increased PAI-1 immunoreactivity was predominantly localized to astrocytes with arteriolar vessels demonstrating PAI-1 immunoreactivity of astrocytic processes adjacent to endothelial cells.

Although there are no previous characterizations of plasmin activity in a rat model of acute OP intoxication, previous studies in rodent models of stroke, systemic inflammation, and Alzheimer's disease report increased levels of active plasmin that promote neuroinflammation [7, 8, 74]. These models, including polytrauma and excluding Alzheimer's disease, have previously reported increases in PAI-1 demonstrating a correlation of an increase in PAI-1 with inflammatory conditions [55, 61, 90].

Increased plasma concentrations of active plasmin seen in DFP intoxicated animals could alter fibrinolysis with elevated PAI-1 levels fostering clot formation. However, increased plasmin activation can simultaneously cause excessive clot formation and excessive bleeding. Plasmin degradation of fibrin produces fibrin degradation products (FDPs), which can compete with thrombin to prevent the conversion of fibrinogen to fibrin and thereby inhibit clot formation [78]. In a transgenic mouse model of experimental deep vein thrombosis, increased plasmin activity prevented thrombosis demonstrating a critical role for plasmin in resolving clots in the vasculature [10]. Our laboratory has observed blot clots in the brains of DFP-intoxicated rats on brain MRI and post-mortem (Hobson, Bruun, unpublished observations). This increase in occurrence of thrombosis in DFP-exposed rats corresponds with a reported increased risk of thrombosis in humans exposed to organophosphates [60]. This risk increases further if the affected individual has health issues associated with increased peripheral plasmin activation and PAI-1, including obesity, smoking, and type 2 diabetes [1, 53, 60]. Since we observed increased concentrations of active plasmin, although highly variable, this begs the question of whether the change is attributable to OP exposure or if it's due to seizure activity. There is some epidemiological evidence that OP-exposed patients who did not experience seizures had an

increased thrombotic risk, although there was no measure of any aspects of the PAS such as FDPs or clotting times [60].

Since concentrations of active plasmin were acutely elevated after acute DFP intoxication, our rationale was to characterize the main inhibitor within the vasculature, PAI-1, to assess whether the increase in active plasmin was simply due to a decrease in the main regulator of plasminogen conversion into plasmin. However, this was not the case, as we observed an acute increase in PAI-1 protein concentration in the plasma at 1 DPE and an elevated concentration at 3 DPE. Our observations are consistent with those reported for a mouse model of kainate-induced SE, in which acute increases in PAI-1 mRNA in the heart and brain were observed within 1 DPE [92]. Although protein levels were not measured in that study, mRNA frequently corresponds with protein levels. The increased PAI-1 levels on plasmin activity could be overwhelming the ability of plasmin to function effectively and thus, serving to promote thrombosis within the brain and periphery.

Peripheral activation of the PAS has been associated with activation of PAS components in the CNS [7, 8]. Our characterization of the spatiotemporal profile of the main components within the PAS confirmed that acute DFP intoxication activated plasmin enzyme activity and increased PAI-1 levels in the brain. Previous publications in our lab have shown that OPs activate neuroinflammation, leading to glial activation, neurodegeneration, and oxidative stress [41, 42, 84]. Much of what appears in the literature for PAS characterization has been published by Strickland in rodent models of stroke, systemic inflammation, and Alzheimer's disease [7, 20, 51, 67, 93]. Furthermore, the principal plasmin activator in normal brain, tPA, is secreted with synaptic activity and recycled locally by astrocytes [16]. For these reasons, it was important to characterize the spatiotemporal variations of tPA, uPA, and PAI-1 in the brain [11, 69]. PAS

activators demonstrated moderate regional increases after acute DFP intoxication that corroborates findings in rodent models of kainic acid excitotoxicity, temporal lobe epilepsy, and traumatic brain injury [21, 46, 58]. PAI-1 markedly increased, presumably functioning as an acute regulatory inhibitor in the cortex and hippocampus after DFP intoxication. Previous findings in a mouse model of pilocarpine-induced SE demonstrated significant increases in PAI-1 protein concentrations at 24 hours post exposure [87]. Similarly, we observed significantly elevated levels of PAI-1, as well as the increased expression of the PAS activators tPA and uPA.

We used immunohistochemistry to identify the cell-specificity of PAS upregulation. Unfortunately, we were unable to identify antibodies that would work for tPA and uPA immunohistochemistry despite testing multiple commercially available antibodies. Previous work in a mouse model of kainate induced SE demonstrated transient increases in tPA IHC and the transport of tPA within the brain which could prove problematic for cell specific IHC characterization [80]. Previous publications looking at uPA IHC describe high levels in the developing brain, but low levels of expression in adult rodents [28, 58]. Future studies should address the gap of tPA and uPA IHC by immunohistochemically characterizing tPA, uPA, and PAI-1 in parallel after acute OP intoxication. In contrast, we were able to optimize PAI-1 immunohistochemistry in the rat brain. PAI-1 immunopositive staining was nearly absent in VEH rats, coinciding with previous studies in rodents and humans [5, 83, 86, 89]. However, PAI-1 immunoreactivity was upregulated out to 28 DPE in DFP exposed rats and primarily localized to astrocyte cell bodies and processes. Previous publications *in vitro* [44, 56, 64] and *in vivo* [47, 93] describe PAI-1 immunoreactivity in astrocytes and endothelial cells, in line with our findings. Reactive astrogliosis occurs in the DFP model [41, 77, 79, 84]; however, the role of these PAI-1 positive astrocytes is unknown and should be addressed in future studies. We

suspect that increased PAI-1 expression is located in astrocytic endfeet on endothelial cells. This needs to be validated by additional studies and does this observation identify regions of the BBB that are altered following acute OP intoxication. tPA is known to cross/alter the BBB and is persistently increased after OP intoxication as presented in our results.

TEM suggested that the PAI-1 immunoreactivity observed acutely following DFP exposure corresponded with neuronal ER and mitochondrial stress. While there are no prior TEM studies of the rat brain after acute OP intoxication, our TEM data are consistent with previous studies demonstrating that intoxication with OP pesticides and nerve agents cause significant oxidative stress [39, 41, 59, 72, 91]. Future studies should explore the link between PAI-1 expression in astrocytes and the cellular stress in neurons to determine if there is a cause-effect relationship between PAI-1 upregulation in astrocytes and metabolic stress in neurons.

5. **Conclusion**

This study provided the first spatiotemporal characterization of the PAS in a model of acute OP intoxication. We observed that acute OP intoxication increases PAS activity, evident as increased plasmin activity and increased concentrations of tPA, uPA, and PAI-1 concentrations in the plasma and in the brain. PAI-1 acts as an acute phase response protein while tPA and uPA are chronically increased after acute DFP intoxication, either in response to increases in neuroinflammation or as a compensatory mechanism. Immunohistochemical analyses indicated that PAI-1 is largely restricted to astrocytic subpopulations that express elevated PAI-1 for up to 28 days post-exposure. Future experiments should focus on pharmacologically inhibiting the components of the PAS to elucidate whether the increase in these components is performing a protective or damaging role after acute OP intoxication, and whether this changes over time. The

most significant question to address in future studies is what role PAI-1 plays after acute OP

intoxication, specifically, if PAI-1 plays a neuroprotective role in astrocytes after acute OP

intoxication. Future studies could use pharmacological inhibition to further explore this question.

References

1	Ahmed S, Zimba O, Gasparyan AY (2020) Thrombosis in Coronavirus disease 2019 (COVID-19) through the prism of Virchow's triad. Clin Rheumatol 39: 2529-2543 Doi 10.1007/s10067-020-05275-1

2	Aisina RB, Mukhametova LI (2014) Structure and function of plasminogen/plasmin system. Russian Journal of Bioorganic Chemistry 40: 590-605 Doi 10.1134/S1068162014060028

3	Albe JR, Boyles DA, Walters AW, Kujawa MR, McMillen CM, Reed DS, Hartman AL (2019) Neutrophil and macrophage influx into the central nervous system are inflammatory components of lethal Rift Valley fever encephalitis in rats. PLoS Pathog 15: e1007833 Doi 10.1371/journal.ppat.1007833

4	Andrew PM, Lein PJ (2021) Neuroinflammation as a Therapeutic Target for Mitigating the Long-Term Consequences of Acute Organophosphate Intoxication. Front Pharmacol 12: 674325-674325 Doi 10.3389/fphar.2021.674325

5	Arai Y, Kubota T, Nakagawa T, Kabuto M, Sato K, Kobayashi H (1998) Production of Urokinase-Type Plasminogen Activator (u-PA) and Plasminogen Activator Inhibitor-1 (PAI-1) in Human Brain Tumours. Acta Neurochirurgica 140: 377-386 Doi 10.1007/s007010050112

6	Atsev S, Tomov N (2020) Using antifibrinolytics to tackle neuroinflammation. Neural Regen Res 15: 2203-2206 Doi 10.4103/1673-5374.284979

7	Baker SK, Chen ZL, Norris EH, Revenko AS, MacLeod AR, Strickland S (2018) Blood-derived plasminogen drives brain inflammation and plaque deposition in a mouse model of Alzheimer's disease. Proceedings of the National Academy of Sciences of the United States of America 115: E9687-E9696 Doi 10.1073/pnas.1811172115

8	Baker SK, Chen ZL, Norris EH, Strickland S (2019) Plasminogen mediates communication between the peripheral and central immune systems during systemic immune challenge with lipopolysaccharide. J Neuroinflammation 16: 172 Doi 10.1186/s12974-019-1560-y

9	Baker SK, Strickland S (2020) A critical role for plasminogen in inflammation. Journal of Experimental Medicine 217: Doi 10.1084/jem.20191865

10	Baldwin JF, Sood V, Elfline MA, Luke CE, Dewyer NA, Diaz JA, Myers DD, Wakefield T, Henke PK (2012) The role of urokinase plasminogen activator and plasmin activator inhibitor-1 on vein wall remodeling in experimental deep vein thrombosis. Journal of Vascular Surgery 56: 1089-1097 Doi https://doi.org/10.1016/j.jvs.2012.02.054

11	Basham ME, Seeds NW (2001) Plasminogen expression in the neonatal and adult mouse brain. Journal of Neurochemistry 77: 318-325 Doi https://doi.org/10.1046/j.1471-4159.2001.00239.x

12   Benjamini Y (2010) Discovering the false discovery rate. Journal of the Royal Statistical Society: Series B (Statistical Methodology) 72: 405-416 Doi https://doi.org/10.1111/j.1467-9868.2010.00746.x

13   Björquist P, Brohlin M, Ehnebom J, Ericsson M, Kristiansen C, Pohl G, Deinum J (1994) Plasminogen activator inhibitor type-1 interacts exclusively with the proteinase domain of tissue plasminogen activator. Biochimica et Biophysica Acta (BBA) - Protein Structure and Molecular Enzymology 1209: 191-202 Doi https://doi.org/10.1016/0167-4838(94)90184-8

14   Briens A, Bardou I, Lebas H, Miles LA, Parmer RJ, Vivien D, Docagne F (2017) Astrocytes regulate the balance between plasminogen activation and plasmin clearance via cell-surface actin. Cell Discovery 3: Doi 10.1038/celldisc.2017.1

15   Cap AP (2016) Plasmin: a driver of hemovascular dysfunction. Blood 128: 2375-2376 Doi 10.1182/blood-2016-09-735720

16   Cassé F, Bardou I, Danglot L, Briens A, Montagne A, Parcq J, Alahari A, Galli T, Vivien D, Docagne F (2012) Glutamate controls tPA recycling by astrocytes, which in turn influences glutamatergic signals. The Journal of neuroscience : the official journal of the Society for Neuroscience 32: 5186-5199 Doi 10.1523/JNEUROSCI.5296-11.2012

17   Cavanaugh JE, Neath AA (2019) The Akaike information criterion: Background, derivation, properties, application, interpretation, and refinements. WIREs Computational Statistics 11: e1460 Doi https://doi.org/10.1002/wics.1460

18   Cesari M, Pahor M, Incalzi RA (2010) Plasminogen activator inhibitor-1 (PAI-1): a key factor linking fibrinolysis and age-related subclinical and clinical conditions. Cardiovasc Ther 28: e72-e91 Doi 10.1111/j.1755-5922.2010.00171.x

19   Chavez-Valdez R, Flock DL, Martin LJ, Northington FJ (2016) Endoplasmic reticulum pathology and stress response in neurons precede programmed necrosis after neonatal hypoxia-ischemia. Int J Dev Neurosci 48: 58-70 Doi 10.1016/j.ijdevneu.2015.11.007

20   Chen ZL, Strickland S (1997) Neuronal death in the hippocampus is promoted by plasmin-catalyzed degradation of laminin. Cell 91: 917-925 Doi 10.1016/S0092-8674(00)80483-3

21   Cho E, Lee KJ, Seo J-W, Byun CJ, Chung S-J, Suh DC, Carmeliet P, Koh J-Y, Kim JS, Lee J-Y (2012) Neuroprotection by urokinase plasminogen activator in the hippocampus. Neurobiology of Disease 46: 215-224 Doi https://doi.org/10.1016/j.nbd.2012.01.010

22   Condron M, Rowell S, Dewey E, Anderson T, Lealiiee L, Farrell D, Hinson H (2018) The procoagulant molecule plasminogen activator inhibitor-1 is associated with injury severity and shock in patients with and without traumatic brain injury. J Trauma Acute Care Surg 85: 888-893 Doi 10.1097/TA.0000000000002040

23   Costa LG (2018) Organophosphorus Compounds at 80: Some Old and New Issues. Toxicol Sci 162: 24-35 Doi 10.1093/toxsci/kfx266

24   Council NR (2011) Guide for the Care and Use of Laboratory Animals: Eighth Edition. The National Academies Press, Washington, DC

25   Cunningham O, Campion S, Perry VH, Murray C, Sidenius N, Docagne F, Cunningham C (2009) Microglia and the urokinase plasminogen activator receptor/uPA system in innate brain inflammation. Glia 57: 1802-1814 Doi 10.1002/glia.20892

26   Das R, Ganapathy S, Mahabeleshwar GH, Drumm C, Febbraio M, Jain MK, Plow EF (2013) Macrophage Gene Expression and Foam Cell Formation Are Regulated by

Plasminogen. Circulation 127: 1209-1218 Doi
10.1161/CIRCULATIONAHA.112.001214

27   Del Rosso M, Fibbi G, Pucci M, Margheri F, Serrati S (2008) The plasminogen activation
      system in inflammation. Front Biosci 13: 4667-4686 Doi 10.2741/3032
28   Dent MAR, Sumi Y, Morris RJ, Seeley PJ (1993) Urokinase-type Plasminogen Activator
      Expression by Neurons and Oligodendrocytes During Process Outgrowth in Developing
      Rat Brain. European Journal of Neuroscience 5: 633-647 Doi
      https://doi.org/10.1111/j.1460-9568.1993.tb00529.x
29   Deshpande LS, Carter DS, Blair RE, DeLorenzo RJ (2010) Development of a prolonged
      calcium plateau in hippocampal neurons in rats surviving status epilepticus induced by
      the organophosphate diisopropylfluorophosphate. Toxicol Sci 116: 623-631 Doi
      10.1093/toxsci/kfq157
30   Dijkstra CD, Döpp EA, Joling P, Kraal G (1985) The Heterogeneity of Mononuclear
      Phagocytes in Lymphoid Organs: Distinct Macrophage Subpopulations in Rat
      Recognized by Monoclonal Antibodies ED1, ED2 and ED3. In: Klaus GGB (ed)
      Microenvironments in the Lymphoid System. 409-419 Doi 10.1007/978-1-4613-8_50
31   Eng LF, Ghirnikar RS, Lee YL (2000) Glial fibrillary acidic protein: GFAP-thirty-one
      years (1969-2000). Neurochem Res 25: 1439-1451 Doi 10.1023/a:1007677003387
32   Eren M, Place AT, Thomas PM, Flevaris P, Miyata T, Vaughan DE (2017) PAI-1 is a
      critical regulator of FGF23 homeostasis. Science Advances 3: e1603259 Doi
      10.1126/sciadv.1603259
33   Faul F, Erdfelder E, Lang AG, Buchner A (2007) G*Power 3: a flexible statistical power
      analysis program for the social, behavioral, and biomedical sciences. Behav Res Methods
      39: 175-191 Doi 10.3758/bf03193146
34   Figueiredo TH, Apland JP, Braga MFM, Marini AM (2018) Acute and long-term
      consequences of exposure to organophosphate nerve agents in humans. Epilepsia 59
      Suppl 2: 92-99 Doi 10.1111/epi.14500
35   Flannery BM, Bruun DA, Rowland DJ, Banks CN, Austin AT, Kukis DL, Li Y, Ford
      BD, Tancredi DJ, Silverman JLet al (2016) Persistent neuroinflammation and cognitive
      impairment in a rat model of acute diisopropylfluorophosphate intoxication. J
      Neuroinflammation 13: 267 Doi 10.1186/s12974-016-0744-y
36   Girard RA, Chauhan PS, Tucker TA, Allen T, Kaur J, Jeffers A, Koenig K, Florova G,
      Komissarov AA, Gaidenko TAet al (2019) Increased expression of plasminogen activator
      inhibitor-1 (PAI-1) is associated with depression and depressive phenotype in C57Bl/6J
      mice. Exp Brain Res 237: 3419-3430 Doi 10.1007/s00221-019-05682-0
37   Gorin F (2018) Intracellular Urokinase uPA-PAl-1 Complex: Disruption by Small
      Molecule Targets Hypoxically Programmed Glioma Cells. Open Access Journal of
      Neurology & Neurosurgery 7: Doi 10.19080/OAJNN.2018.07.555712
38   Gorin FA, Pasupuleti N, Dugar DM, Sundeep (2017) Killing Glioma 'Stem-like' Cells
      via Drug-Induced Relocation of Endosomal Urokinase Proteins. 40-47 Doi
      10.2174/1871520616666160628122901
39   Goswami DG, Kant R, Ammar DA, Agarwal C, Gomez J, Agarwal R, Saba LM, Fritz
      KS, Tewari-Singh N (2020) Toxic consequences and oxidative protein carbonylation
      from chloropicrin exposure in human corneal epithelial cells. Toxicology Letters 322: 1-
      11 Doi https://doi.org/10.1016/j.toxlet.2019.12.023

40   Griemert EV, Recarte Pelz K, Engelhard K, Schafer MK, Thal SC (2019) PAI-1 but Not PAI-2 Gene Deficiency Attenuates Ischemic Brain Injury After Experimental Stroke. Transl Stroke Res 10: 372-380 Doi 10.1007/s12975-018-0644-9

41   Guignet M, Dhakal K, Flannery BM, Hobson BA, Zolkowska D, Dhir A, Bruun DA, Li S, Wahab A, Harvey DJet al (2020) Persistent behavior deficits, neuroinflammation, and oxidative stress in a rat model of acute organophosphate intoxication. Neurobiol Dis 133: 104431 Doi 10.1016/j.nbd.2019.03.019

42   Guignet M, Lein PJ (2019) Chapter Two - Neuroinflammation in organophosphate-induced neurotoxicity. In: Aschner M, Costa LG (eds) Advances in Neurotoxicology. Academic Press, Cambridge, MA, pp 35-79

43   Gur-Wahnon D, Mizrachi T, Maaravi-Pinto FY, Lourbopoulos A, Grigoriadis N, Higazi AAR, Brenner T (2013) The plasminogen activator system: Involvement in central nervous system inflammation and a potential site for therapeutic intervention. Journal of Neuroinflammation 10: 891-891 Doi 10.1186/1742-2094-10-124

44   Handt S, Jerome WG, Tietze L, Hantgan RR (1996) Plasminogen Activator Inhibitor-1 Secretion by Endothelial Cells Increases Fibrinolytic Resistance of an In Vitro Fibrin Clot: Evidence for a Key Role of Endothelial Cells in Thrombolytic Resistance. Blood 87: 4204-4213 Doi https://doi.org/10.1182/blood.V87.10.4204.bloodjournal87104204

45   Harbeck N, Schmitt M, Meisner C, Friedel C, Untch M, Schmidt M, Sweep CGJ, Lisboa BW, Lux MP, Beck Tet al (2013) Ten-year analysis of the prospective multicentre Chemo-N0 trial validates American Society of Clinical Oncology (ASCO)-recommended biomarkers uPA and PAI-1 for therapy decision making in node-negative breast cancer patients. https://doi.org/10.1016/j.ejca.2013.01.007

46   Hijazi N, Abu Fanne R, Abramovitch R, Yarovoi S, Higazi M, Abdeen S, Basheer M, Maraga E, Cines DB, Al-Roof Higazi A (2015) Endogenous plasminogen activators mediate progressive intracerebral hemorrhage after traumatic brain injury in mice. Blood 125: 2558-2567 Doi 10.1182/blood-2014-08-588442

47   Hino H, Akiyama H, Iseki E, Kato M, Kondo H, Ikeda K, Kosaka K (2001) Immunohistochemical localization of plasminogen activator inhibitor-1 in rat and human brain tissues. Neuroscience Letters 297: 105-108 Doi https://doi.org/10.1016/S0304-3940(00)01679-7

48   Hohensinner PJ, Baumgartner J, Kral-Pointner JB, Uhrin P, Ebenbauer B, Thaler B, Doberer K, Stojkovic S, Demyanets S, Fischer MBet al (2017) PAI-1 (Plasminogen Activator Inhibitor-1) Expression Renders Alternatively Activated Human Macrophages Proteolytically Quiescent. Arterioscler Thromb Vasc Biol 37: 1913-1922 Doi 10.1161/ATVBAHA.117.309383

49   Horrevoets AJG (2004) Plasminogen activator inhibitor 1 (PAI-1): In vitro activities and clinical relevance. doi: 10.1111/j.1365-2141.2004.04844.x.

50   Hultman K, Blomstrand F, Nilsson M, Wilhelmsson U, Malmgren K, Pekny M, Kousted T, Jern C, Tjarnlund-Wolf A (2010) Expression of plasminogen activator inhibitor-1 and protease nexin-1 in human astrocytes: Response to injury-related factors. J Neurosci Res 88: 2441-2449 Doi 10.1002/jnr.22412

51   Hultman K, Cortes-Canteli M, Bounoutas A, Richards AT, Strickland S, Norris EH (2014) Plasmin deficiency leads to fibrin accumulation and a compromised inflammatory response in the mouse brain. Journal of Thrombosis and Haemostasis 12: 701-712 Doi 10.1111/jth.12553

52   Jett DA, Sibrizzi CA, Blain RB, Hartman PA, Lein PJ, Taylor KW, Rooney AA (2020) A national toxicology program systematic review of the evidence for long-term effects after acute exposure to sarin nerve agent. Critical Reviews in Toxicology 50: 474-490 Doi 10.1080/10408444.2020.1787330

53   Ji H-L, Zhao R, Matalon S, Matthay MA (2020) Elevated Plasmin(ogen) as a Common Risk Factor for COVID-19 Susceptibility. Physiol Rev 100: 1065-1075 Doi 10.1152/physrev.00013.2020

54   Kim Y-B, Hur G-H, Shin S, Sok D-E, Kang J-K, Lee Y-S (1999) Organophosphate-induced brain injuries: delayed apoptosis mediated by nitric oxide. Environmental Toxicology and Pharmacology 7: 147-152 Doi https://doi.org/10.1016/S1382-6689(99)00006-X

55   Kluft C, de Bart ACW, Barthels M, Sturm J, Möller W (1988) Short term extreme increases in plasminogen activator inhibitor 1 (PAI-1) in plasma of polytrauma patients. Fibrinolysis 2: 223-226 Doi https://doi.org/10.1016/0268-9499(88)90017-3

56   Kollros PR, Konkle BA, Ambarian AP, Henrikson P (1994) Plasminogen Activator Inhibitor-1 Expression by Brain Microvessel Endothelial Cells Is Inhibited by Elevated Glucose. Journal of Neurochemistry 63: 903-909 Doi https://doi.org/10.1046/j.1471-4159.1994.63030903.x

57   Kruger LS, Samuel; Swanson, Larry (1995) Photographic Atlas of the Rat Brain. Cambridge University Press, Cambridge, MA

58   Lahtinen L, Lukasiuk K, Pitkänen A (2006) Increased expression and activity of urokinase-type plasminogen activator during epileptogenesis. European Journal of Neuroscience 24: 1935-1945 Doi https://doi.org/10.1111/j.1460-9568.2006.05062.x

59   Liang L-P, Pearson-Smith JN, Huang J, McElroy P, Day BJ, Patel M (2018) Neuroprotective Effects of AEOL10150 in a Rat Organophosphate Model. Toxicol Sci 162: 611-621 Doi 10.1093/toxsci/kfx283

60   Lim Y-P, Lin C-L, Hung D-Z, Ma W-C, Lin Y-N, Kao C-H (2015) Increased risk of deep vein thrombosis and pulmonary thromboembolism in patients with organophosphate intoxication: a nationwide prospective cohort study. Medicine (Baltimore) 94: e341-e341 Doi 10.1097/MD.0000000000000341

61   Lip GYH, Blann AD, Farooqi IS, Zarifis J, Sagar G, Beevers DG (2002) Sequential alterations in haemorheology, endothelial dysfunction, platelet activation and thrombogenesis in relation to prognosis following acute stroke: The West Birmingham Stroke Project. Blood Coagulation & Fibrinolysis Doi 10.1097/00001721-200206000-00010

62   Liu B, Zhang B, Wang T, Liang QC, Jing XR, Zheng J, Wang C, Meng Q, Wang L, Wang Wet al (2010) Increased expression of urokinase-type plasminogen activator receptor in the frontal cortex of patients with intractable frontal lobe epilepsy. J Neurosci Res 88: 2747-2754 Doi 10.1002/jnr.22419

63   Liu RM, van Groen T, Katre A, Cao D, Kadisha I, Ballinger C, Wang L, Carroll SL, Li L (2011) Knockout of plasminogen activator inhibitor 1 gene reduces amyloid beta peptide burden in a mouse model of Alzheimer's disease. Neurobiology of Aging 32: 1079-1089 Doi 10.1016/j.neurobiolaging.2009.06.003

64   Liu Y, Honda S, Kohsaka S, Nakajima K (2000) Plasminogen enhances the secretion of plasminogen activator inhibitor-1 from cultured rat astrocytes. Neuroscience Letters 282: 137-140 Doi https://doi.org/10.1016/S0304-3940(00)00860-0

65   Lyck L, Dalmau I, Chemnitz J, Finsen B, Schroder HD (2008) Immunohistochemical markers for quantitative studies of neurons and glia in human neocortex. J Histochem Cytochem 56: 201-221 Doi 10.1369/jhc.7A7187.2007

66   Mehra A, Ali C, Parcq J, Vivien D, Docagne F (2016) The plasminogen activation system in neuroinflammation. Biochimica et Biophysica Acta (BBA) - Molecular Basis of Disease 1862: 395-402 Doi https://doi.org/10.1016/j.bbadis.2015.10.011

67   Melchor JP, Pawlak R, Strickland S (2003) The tissue plasminogen activator-plasminogen proteolytic cascade accelerates amyloid-beta (Abeta) degradation and inhibits Abeta-induced neurodegeneration. The Journal of neuroscience : The Official Journal of the Society for Neuroscience 23: 8867-8871 Doi 10.1523/JNEUROSCI.23-26-08867.2003

68   Melchor JP, Strickland S (2005) Tissue plasminogen activator in central nervous system physiology and pathology. Thromb Haemost 93: 655-660 Doi 10.1160/TH04-12-0838

69   Mindel E, Weiss R, Bushi D, Gera O, Orion D, Chapman J, Shavit-Stein E (2021) Increased brain plasmin levels following experimental ischemic stroke in male mice. Journal of Neuroscience Research 99: 966-976 Doi https://doi.org/10.1002/jnr.24764

70   Oh J, Lee HJ, Song JH, Park SI, Kim H (2014) Plasminogen activator inhibitor-1 as an early potential diagnostic marker for Alzheimer's disease. Exp Gerontol 60: 87-91 Doi 10.1016/j.exger.2014.10.004

71   Pasupuleti N, Grodzki AC, Gorin F (2015) Mis-trafficking of endosomal urokinase proteins triggers drug-induced glioma nonapoptotic cell death. Mol Pharmacol 87: 683-696 Doi 10.1124/mol.114.096602

72   Pearson JN, Patel M (2016) The role of oxidative stress in organophosphate and nerve agent toxicity. Annals of the New York Academy of Sciences 1378: 17-24 Doi 10.1111/nyas.13115

73   Pereira EFR, Aracava Y, DeTolla LJ, Jr., Beecham EJ, Basinger GW, Jr., Wakayama EJ, Albuquerque EX (2014) Animal models that best reproduce the clinical manifestations of human intoxication with organophosphorus compounds. J Pharmacol Exp Ther 350: 313-321 Doi 10.1124/jpet.114.214932

74   Pfefferkorn T, Staufer B, Liebetrau M, Bültemeier G, Vosko MR, Zimmermann C, Hamann GF (2000) Plasminogen Activation in Focal Cerebral Ischemia and Reperfusion. Journal of Cerebral Blood Flow & Metabolism 20: 337-342 Doi 10.1097/00004647-200002000-00015

75   Podor TJ, Peterson CB, Lawrence DA, Stefansson S, Shaughnessy SG, Foulon DM, Butcher M, Weitz JI (2000) Type 1 plasminogen activator inhibitor binds to fibrin via vitronectin. J Biol Chem 275: 19788-19794 Doi 10.1074/jbc.M908079199

76   Pouliot W, Bealer SL, Roach B, Dudek FE (2016) A rodent model of human organophosphate exposure producing status epilepticus and neuropathology. NeuroToxicology 56: 196-203 Doi https://doi.org/10.1016/j.neuro.2016.08.002

77   Putra M, Gage M, Sharma S, Gardner C, Gasser G, Anantharam V, Thippeswamy T (2020) Diapocynin, an NADPH oxidase inhibitor, counteracts diisopropylfluorophosphate-induced long-term neurotoxicity in the rat model. Annals of the New York Academy of Sciences 1479: 75-93 Doi https://doi.org/10.1111/nyas.14314

78   Rijken DC, Sakharov DV (2001) Basic Principles in Thrombolysis: Regulatory Role of Plasminogen. Thrombosis Research 103: S41-S49 Doi https://doi.org/10.1016/S0049-3848(01)00296-1

79   Rojas A, Ganesh T, Lelutiu N, Gueorguieva P, Dingledine R (2015) Inhibition of the prostaglandin EP2 receptor is neuroprotective and accelerates functional recovery in a rat model of organophosphorus induced status epilepticus. Neuropharmacology 93: 15-27 Doi https://doi.org/10.1016/j.neuropharm.2015.01.017

80   Sallés FJ, Strickland S (2002) Localization and Regulation of the Tissue Plasminogen Activator–Plasmin System in the Hippocampus. The Journal of Neuroscience 22: 2125 Doi 10.1523/JNEUROSCI.22-06-02125.2002

81   Schmitt M, Mengele K, Napieralski R, Magdolen V, Reuning U, Gkazepis A, Sweep F, Brünner N, Foekens J, Harbeck N (2010) Clinical utility of level-of-evidence-1 disease forecast cancer biomarkers uPA and its inhibitor PAI-1. Expert Review of Molecular Diagnostics 10: https://doi.org/10.1586/ERM.10.71

82   Schuliga M (2015) The Inflammatory Actions of Coagulant and Fibrinolytic Proteases in Disease. Mediators of Inflammation 2015: 437695 Doi 10.1155/2015/437695

83   Simpson AJ, Booth NA, Moore NR, Bennett B (1991) Distribution of plasminogen activator inhibitor (PAI-1) in tissues. Journal of Clinical Pathology 44: 139 Doi 10.1136/jcp.44.2.139

84   Siso S, Hobson BA, Harvey DJ, Bruun DA, Rowland DJ, Garbow JR, Lein PJ (2017) Editor's Highlight: Spatiotemporal Progression and Remission of Lesions in the Rat Brain Following Acute Intoxication With Diisopropylfluorophosphate. Toxicol Sci 157: 330-341 Doi 10.1093/toxsci/kfx048

85   Sutton R, Keohane ME, VanderBerg SR, Gonias SL (1994) Plasminogen activator inhibitor-1 in the cerebrospinal fluid as an index of neurological disease. Blood Coagul Fibrinolysis 5: 167-171 Doi 10.1097/00001721-199404000-00002

86   Tang M, Jiang P, Li H, Cai H, Liu Y, Gong H, Zhang L (2015) Antidepressant-like effect of n-3 PUFAs in CUMS rats: role of tPA/PAI-1 system. Physiology & Behavior 139: 210-215 Doi https://doi.org/10.1016/j.physbeh.2014.11.054

87   Thomas AX, Cruz Del Angel Y, Gonzalez MI, Carrel AJ, Carlsen J, Lam PM, Hempstead BL, Russek SJ, Brooks-Kayal AR (2016) Rapid Increases in proBDNF after Pilocarpine-Induced Status Epilepticus in Mice Are Associated with Reduced proBDNF Cleavage Machinery. eNeuro 3: ENEURO.0020-0015.2016 Doi 10.1523/ENEURO.0020-15.2016

88   Tian GH, Sun K, Huang P, Zhou CM, Yao HJ, Huo ZJ, Hao HF, Yang L, Pan CS, He Ket al (2013) Long-Term Stimulation with Electroacupuncture at DU20 and ST36 Rescues Hippocampal Neuron through Attenuating Cerebral Blood Flow in Spontaneously Hypertensive Rats. Evid Based Complement Alternat Med 2013: 482947 Doi 10.1155/2013/482947

89   Tsantarliotou MP, Lavrentiadou SN, Psalla DA, Margaritis IE, Kritsepi MG, Zervos IA, Latsari MI, Sapanidou VG, Taitzoglou IA, Sinakos ZM (2019) Suppression of plasminogen activator inhibitor-1 (PAI-1) activity by crocin ameliorates lipopolysaccharide-induced thrombosis in rats. Food and Chemical Toxicology 125: 190-197 Doi https://doi.org/10.1016/j.fct.2019.01.001

90   Ueda S, Nishio K, Minamino N, Kubo A, Akai Y, Kangawa K, Matsuo H, Fujimura Y, Yoshioka A, Masui Ket al (1999) Increased Plasma Levels of Adrenomedullin in Patients with Systemic Inflammatory Response Syndrome. American Journal of Respiratory and Critical Care Medicine 160: 132-136 Doi 10.1164/ajrccm.160.1.9810006

91   Vanova N, Pejchal J, Herman D, Dlabkova A, Jun D (2018) Oxidative stress in organophosphate poisoning: role of standard antidotal therapy. Journal of Applied Toxicology 38: 1058-1070 Doi https://doi.org/10.1002/jat.3605

92   Venugopal B, Sharon R, Abramovitz R, Khasin A, Miskin R (2001) Plasminogen activator inhibitor-1 in cardiovascular cells: rapid induction after injecting mice with kainate or adrenergic agents. Cardiovascular Research 49: 476-483 Doi 10.1016/S0008-6363(00)00271-6

93   Wang YF, Tsirka SE, Strickland S, Stieg PE, Soriano SG, Lipton SA (1998) Tissue plasminogen activator (tPA) increases neuronal damage after focal cerebral ischemia in wild-type and tPA-deficient mice. Nat Med 4: 228-231 Doi 10.1038/nm0298-228

Table 1: Distribution of animals across study endpoints.

Cohort	Endpoints Evaluated	Tissue used	Sample Size	Figures
1 N=38 DFP N=19 VEH	Seizure behavior Immunohistochemistry ELISAs Plasmin Activity Assay	Coronal Brain Sections Plasma, Cerebellum, Cortex, Hippocampus Plasma	38/38 DFP, 19/19 VEH 11-12/38 DFP, 11-12/19 VEH 30-36/38 DFP, 14-17/19 VEH 16/38 DFP, 15/19 VEH	2c 7, 8, 9, 10, 11 5, 6 4
2	Transmission Electron Microscopy	Coronal Brain Sections	2 (1 DFP, 1 VEH)	3

Table 2: List of primary antibodies used for immunohistochemistry

1° Antibody	Host	Source	Location	Product #	Lot #	Dilution	Clonality	Clone	Subclass	RRID
Anti-NeuN	Mouse	Millipore	Burlington, MA, USA	MAB377	2919676	1:500	Mono	A60	IgG1	AB_2298772
Anti-rat Cd68	Mouse	Bio-Rad	Hercules, CA, USA	MCA341R	148924C	1:200	Mono	ED1	IgG1	AB_2291300
Anti-GFAP	Mouse	Cell Signaling	Danvers, MA, USA	3670	6	1:1000	Mono	GA5	IgG1	AB_561049
Anti AIF/Iba1	Goat	Novus	Centennial, CO, USA	NB1001028	S7C7G2P40	1:500	Poly	N/A	N/A	AB_521594
Anti-PAI-1	Rabbit	MyBioSource	San Diego, CA, USA	MBS1265040	F0928A	1:100 IHC 1:1000 WB	Poly	N/A	IgG	N/A
Anti-CD31	Mouse	Thermo Fisher	Waltham, MA, USA	MA180069	WB3189522, WB3186081B	1:50	Mono	TLD-3A12	IgG1	AB_928130

Table 3: List of secondary antibodies used for immunohistochemistry

2° Antibody	Host	Reacts with	Source	Product #	Lot #	Dilution	Wavelength	Antibody used with	RRID
Anti-Rabbit IgG (H+L)	Goat	Rabbit	Invitrogen	A21245	2299231	1:600	647	PAI-1	AB_2535813
Anti-mouse IgG1 Alexa Fluor	Goat	Mouse	Invitrogen	A21124	2300937	1:1000	568	GFAP, NeuN	AB_2535766
Anti-mouse AlexaFluor	Goat	Mouse	Invitrogen	A21121	2271701	1:1000	488	Cd31	AB_2535764
Anti-goat F(ab)2	Donkey	Goat	Jackson ImmunoResearch	705606147	144080	1:500	647	Iba1	AB_2340438
Anti-rabbit H+L AlexaFluor	Donkey	Rabbit	Invitrogen	A10042	2207536	1:600	568	PAI-1	AB_2534017
Anti-mouse IgG	Donkey	Mouse	Invitrogen	A21202	2147618	1:1000	488	Cd68	AB_141607
Anti-rabbit IgG	Goat	Rabbit	Licor	926-68071	C80605-15	1:10000	680	PAI-1	AB_10956166

Figures and Figure Legends
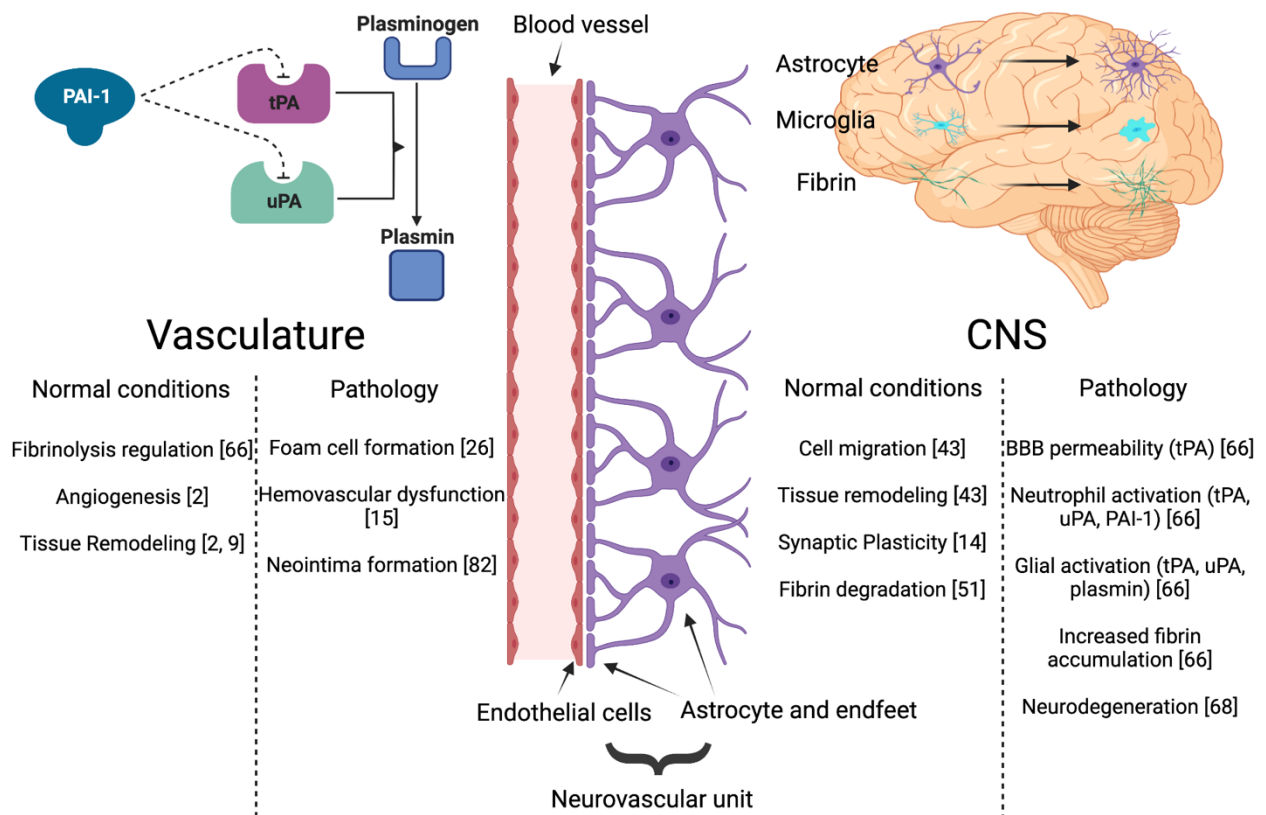
Fig. 1 The roles and pathologies associated with the plasminogen activation system in the periphery and central nervous system (CNS). The upper left of the diagram represents an overview of the enzymatic cascade in which the precursor, plasminogen, is cleaved by tissue plasminogen activator (tPA) and urokinase plasminogen activator (uPA) to the active serine protease, plasmin. Plasminogen activator inhibitor-1 (PAI-1) functions to inhibit the enzymatic activity of tPA and uPA, thereby preventing the activation of plasminogen. The upper right of the diagram represents cellular and molecular components that are critically involved in neuroinflammatory responses in the brain. These include astrocytes (purple), microglia (turquoise) and fibrin (green). The left side of the brain represents the normal physiologic state; the right, neuroinflammation.
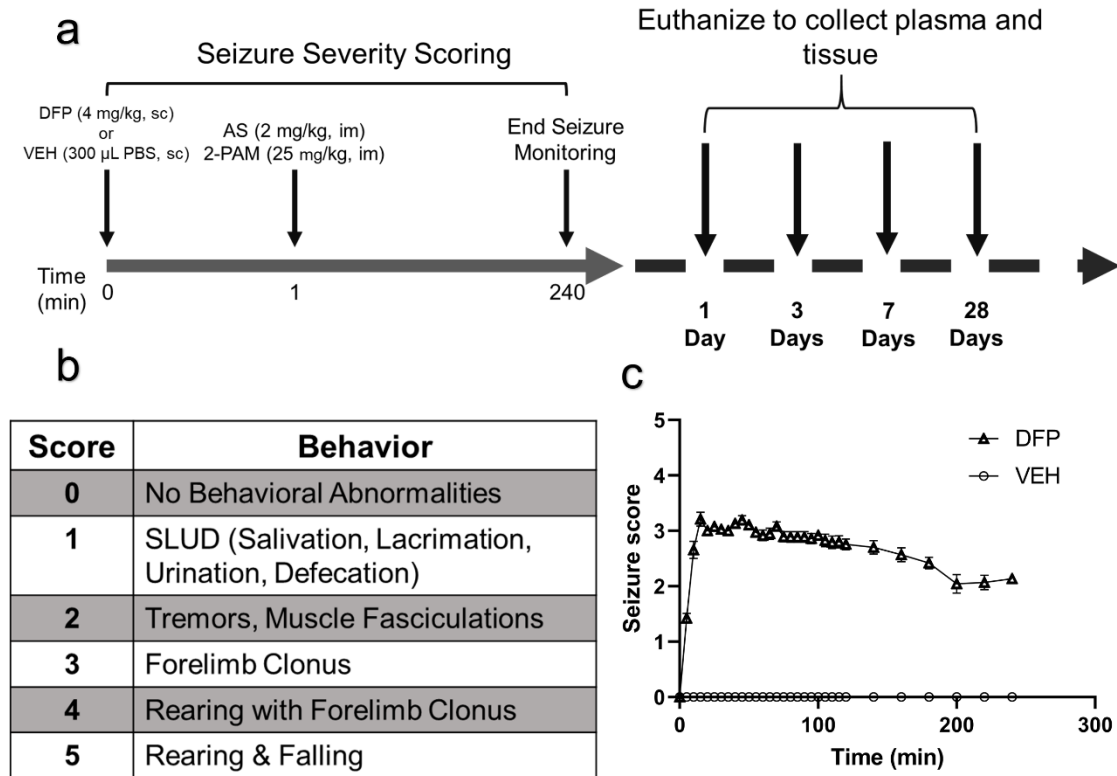
Fig. 2 The rat model of acute DFP intoxication. a Schematic illustrating the dosing paradigm used to trigger DFP-induced seizures in adult male Sprague-Dawley rats and timeline of data collection. **b** Scale used to score seizure behavior in DFP-intoxicated rats. **c** Profile of seizure scores in DFP and VEH animals. Data presented as mean ± SE (DFP n=38, VEH n=19)

	Hippocampus	Piriform Cortex
VEH		
DFP		
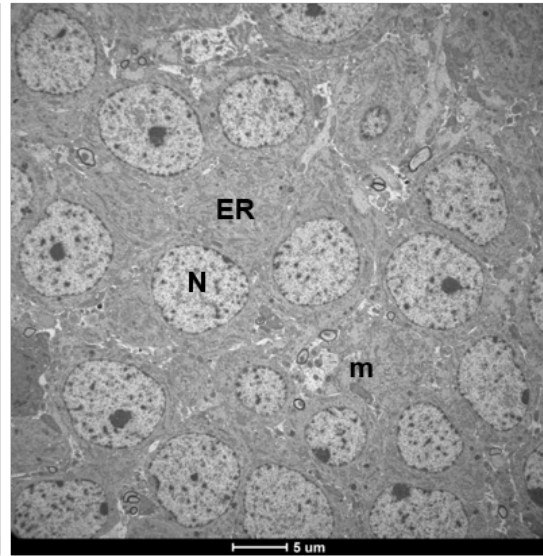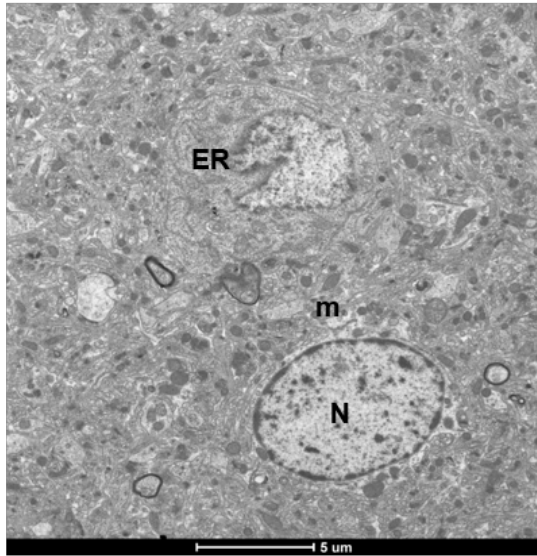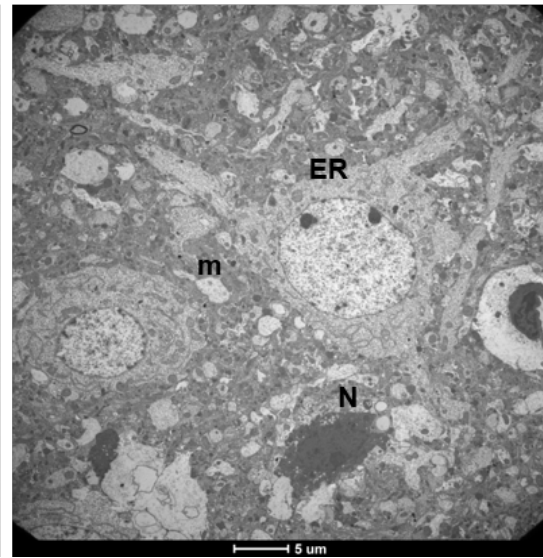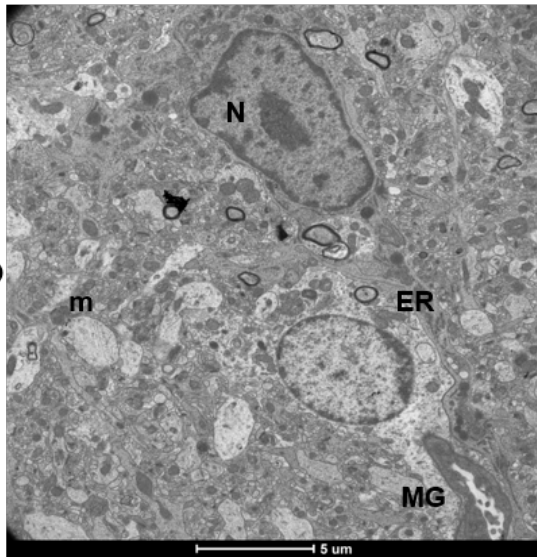
Fig. 3 Representative transmission electron micrographs of 1-day post-DFP and time-matched vehicle (VEH) control of the DG of the hippocampus and piriform cortex. Early neurodegeneration is evident in both the hippocampus and piriform cortex of DFP-exposed animals as indicated by mitochondrial abnormalities (m). Dark neurons (N) and microglia (MG) are suggestive of oxidative injury compared to VEH. Dilation of the endoplasmic reticulum (ER) and ribosomal detachment may represent a manifestation of acute, generalized neuronal dysfunction compounded by oxidative stress. VEH samples show no indication of oxidative injury, mitochondrial abnormalities (m), endoplasmic reticulum stress (er), nor early neurodegeneration (N)
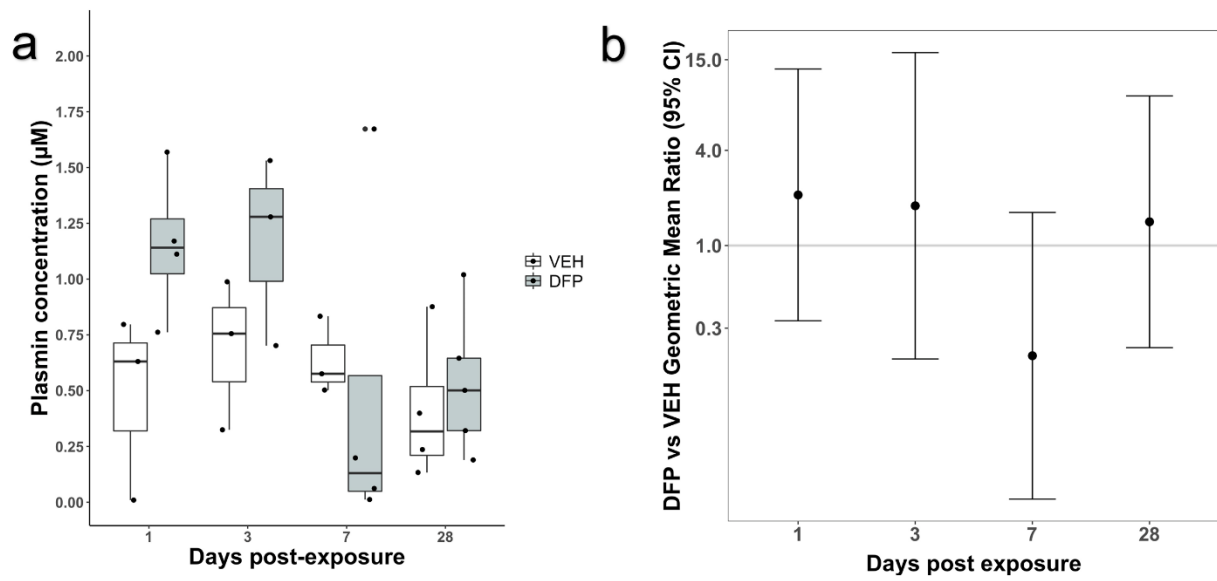
Fig. 4 Temporal changes in active plasmin concentrations in VEH and DFP animals. **a** Data are presented as box plots of VEH (n=3-5) and DFP-exposed animals (n=3-5) for each time point. The box plot bounds represent the interquartile range (IQR) divided by the median, the line within the box, and the whiskers extend 1.5 x the IQR. **b** Total active plasmin levels geometric mean ration (GMR) with 95% CI at 1, 3, 7, and 28-day post-exposure in DFP versus VEH animals. A GMR with a 95% CI that crosses the 1.0 intercept indicates no significant difference. A GMR with a 95% CI above or below the 1.0 intercept indicates a significant increase or decrease, respectively. Blue CIs indicate significant differences between DFP and VEH groups (p<0.05)
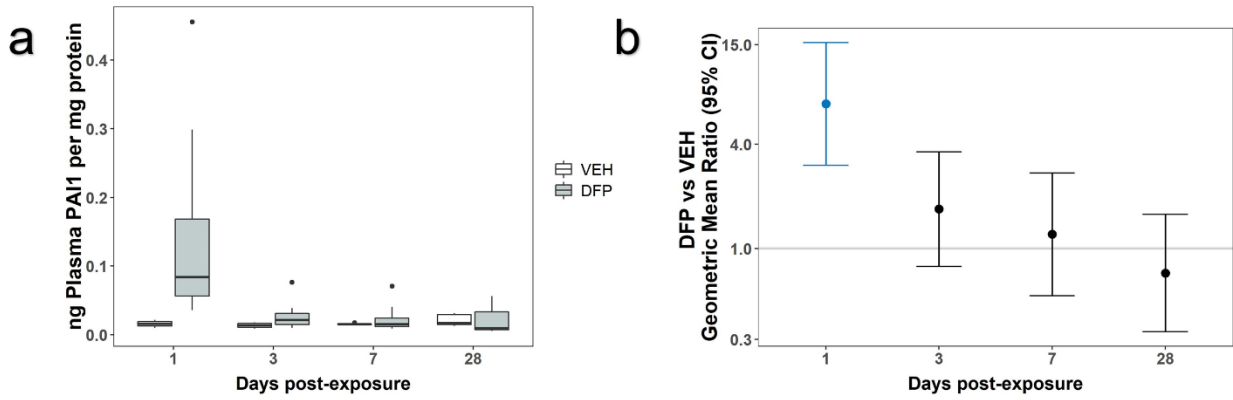
Fig. 5 Temporal pattern of plasma PAI-1 levels. **a** Temporal changes in plasma PAI-1 levels in VEH and DFP animals. Data are presented as box plots of VEH (n=4-5) and DFP-exposed animals (n=7-13) for each time point. The box plot bounds represent the interquartile range (IQR) divided by the median, the line within the box, and the whiskers extend 1.5 x the IQR. **b** Total Plasma PAI-1 geometric mean ration (GMR) with 95% CI at 1, 3, 7, and 28-day post-exposure in DFP versus VEH animals. A GMR with a 95% CI that crosses the 1.0 intercept indicates no significant difference. A GMR with a 95% CI above or below the 1.0 intercept indicates a significant increase or decrease, respectively. Blue CIs indicate significant differences between DFP and VEH groups ($p<0.05$)
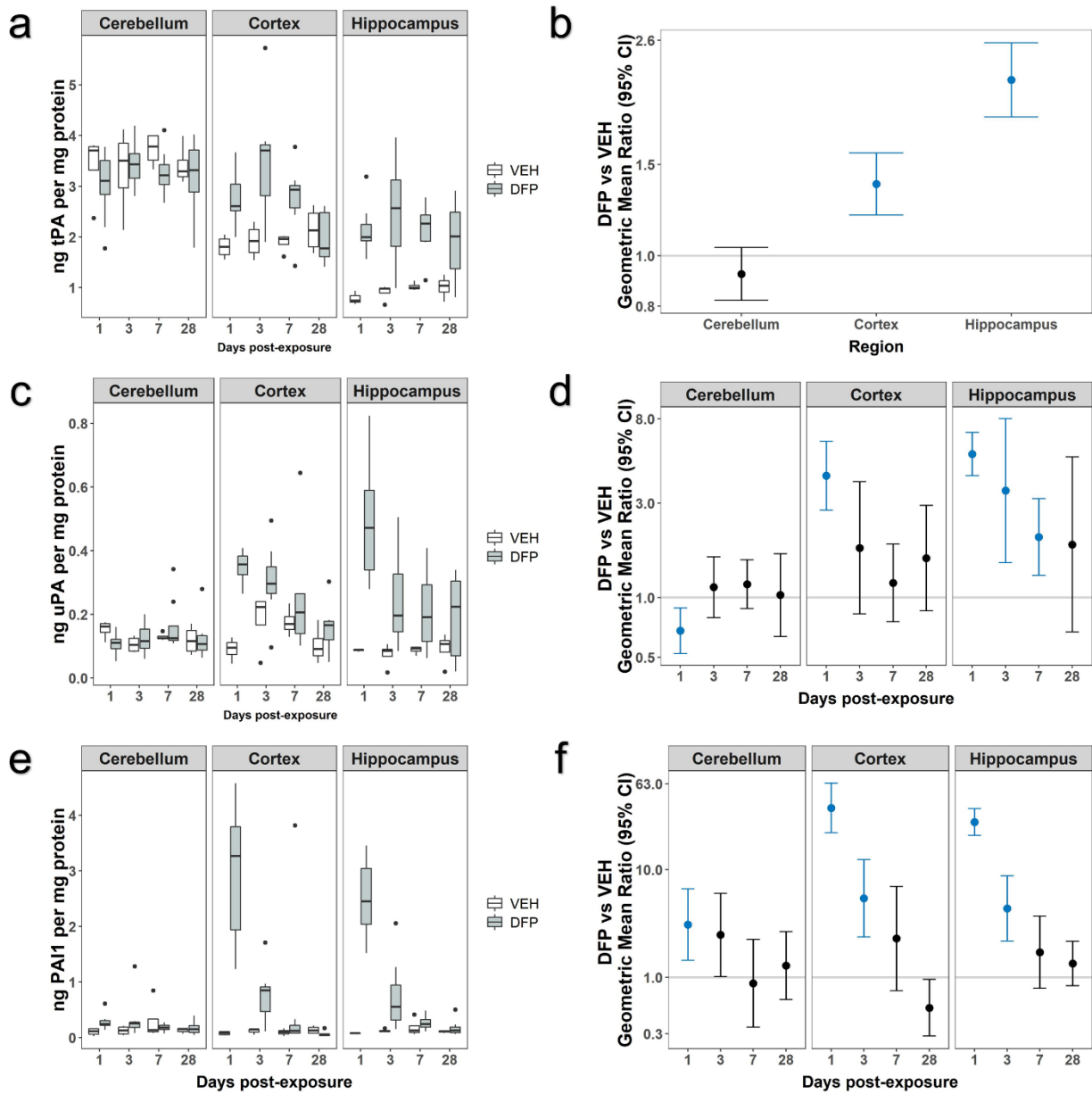
Fig. 6 Acute DFP intoxication increases brain levels of proteins in the plasmin system in a region-dependent

manner. **a** Spatiotemporal brain expression of tPA in VEH (n=3-4) vs. DFP (n=7-9) animals. The box plot bounds

represent the interquartile range (IQR) divided by the median, the line within the box, and the whiskers extend 1.5 x

the IQR. **b** DFP versus VEH tPA geometric mean ratio (GMR) with 95% CI at 1, 3, 7, and 28 days post-exposure.

There was no difference in the tPA exposure effect by time point, so estimates of group differences were averaged

across time points. **c** Spatiotemporal brain expression of uPA levels in VEH (n=3-4) and DFP (n=7-9) animals. The

box plot bounds represent the interquartile range (IQR) divided by the median, the line within the box, and the whiskers extend 1.5 x the IQR. **d** DFP versus VEH uPA GMR with 95% CI at 1, 3, 7, and 28-day post-exposure. **e** Spatiotemporal brain expression of PAI-1 levels in VEH (n=3-4) and DFP (n=7-9) animals. The box plot bounds represent the interquartile range (IQR) divided by the median, the line within the box, and the whiskers extend 1.5 x the IQR. **f** DFP versus VEH PAI-1 GMR with 95% CI in 1, 3, 7, and 28 day post-exposure. In panels **b**, **d** and **f**, CIs in blue indicate significant results (p<0.05). A GMR with a 95% CI that crosses the 1.0 intercept indicates no significant difference between groups. A GMR with a 95% CI above or below the 1.0 intercept indicates a significant increase or decrease, respectively
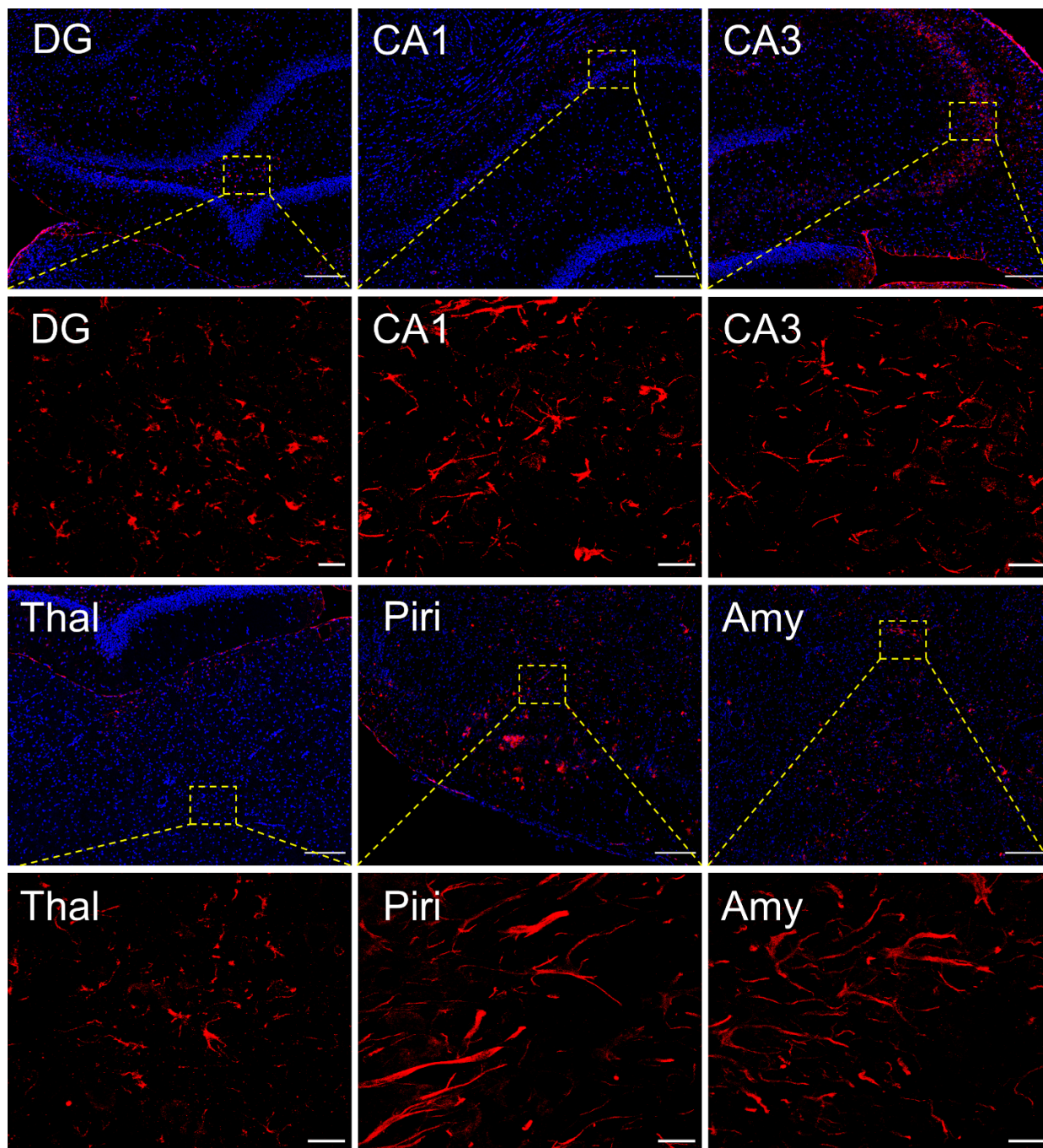
**Fig. 7** Acute DFP intoxication induces PAI-1 expression in all brain regions at 28 days post-exposure. The area in the dotted yellow box is shown at higher magnification in the image below. Representative photomicrographs of PAI-1 immunoreactivity (red). Sections were counterstained with DAPI (blue) to identify cell nuclei. Low magnification bars= 200 μm and high magnification bars= 20 μm
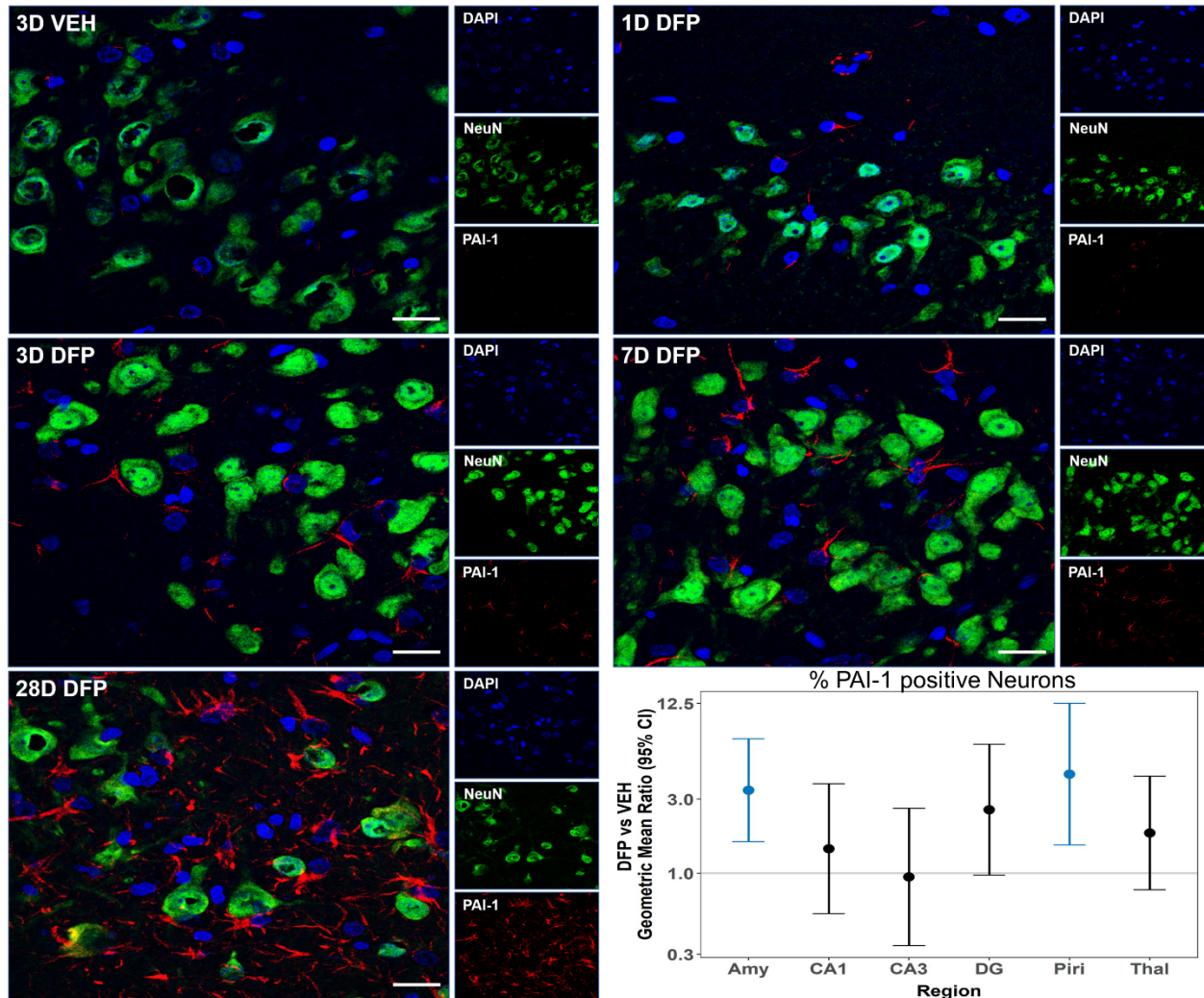
Fig. 8 DFP-induced PAI-1 expression is excluded from hippocampal neurons. Representative photomicrographs the hilus of the hippocampus at 1, 3, 7 and 28 days post-exposure of a VEH and DFP animal co-immunostained for PAI-1 (red) and NeuN (green). Sections were counterstained with DAPI to identify cell nuclei. Bar represents 20 μm. Regional PAI-1 and NeuN colocalization geometric mean ration (GMR) with 95% CI in DFP (n=10-12) versus VEH (n=10-12) animals. There was no difference in the colocalization effect by time point, so estimates of group differences were averaged across time points. Acute DFP intoxication induces PAI-1 expression but not colocalization in neurons. A GMR with a 95% CI that crosses the 1.0 intercept indicates no significant difference between groups. A GMR with a blue 95% CI above or below the 1.0 intercept indicates a significant increase or decrease (p<0.05), respectively
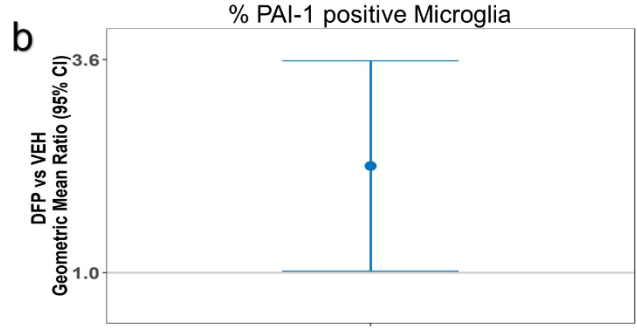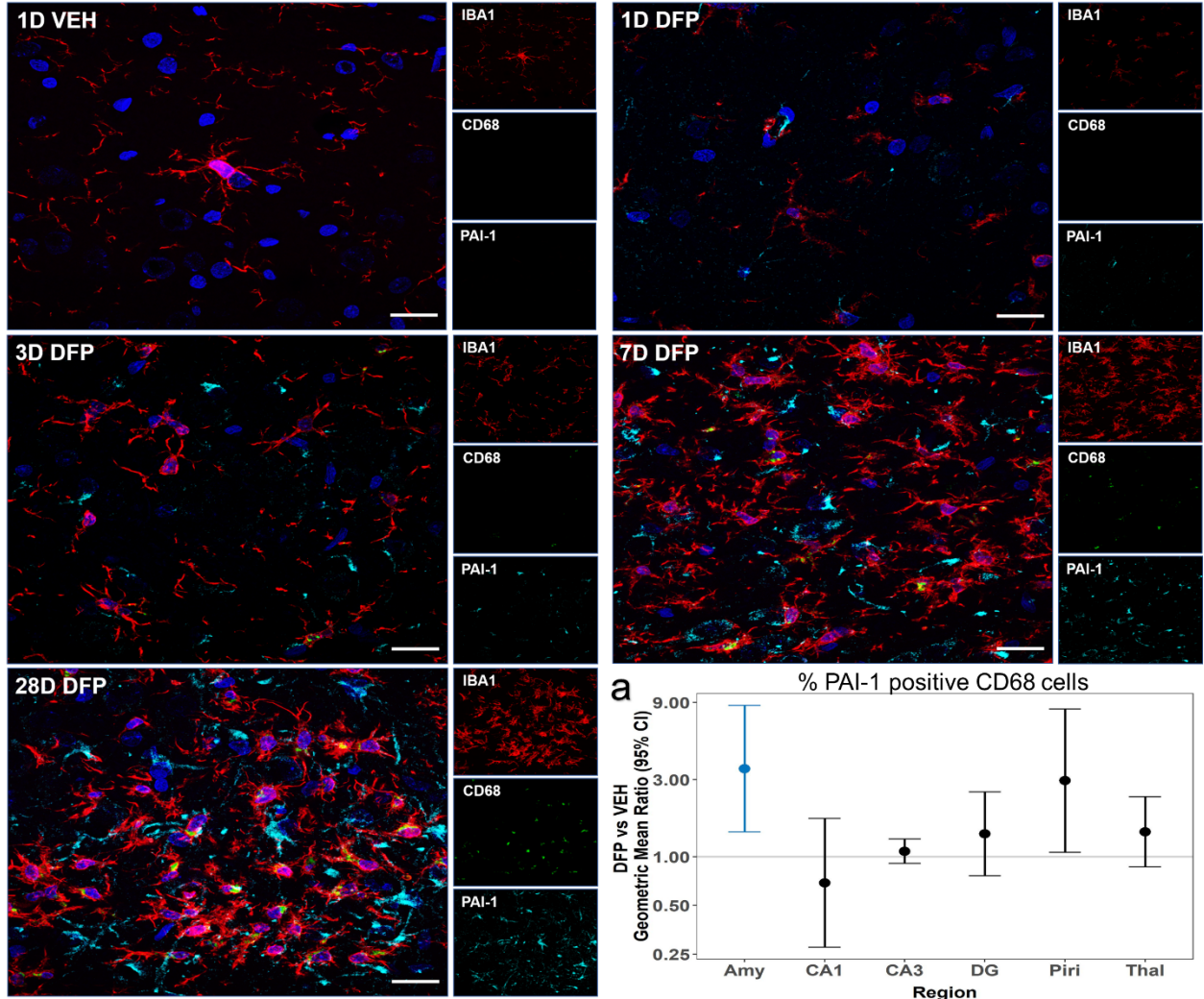
Fig. 9 DFP-induced PAI-1 expression is largely excluded from CD68 positive glia and microglial cells. Representative photomicrographs of VEH animal compared to DFP animals IBA1 (red), CD68 (green), and PAI-1 (cyan) immunoreactivity in the hilus of the hippocampus at 1, 3, 7 and 28 days post-exposure. Sections were counterstained with DAPI (blue) to identify cell nuclei. Bar represents 20 µm. **a** Regional PAI-1 and CD68 colocalization geometric mean ration (GMR) with 95% CI in DFP (n=10-12) versus VEH (n=10-12) animals. There was no difference in the colocalization effect by time point, so estimates of group differences were averaged across time points. Acute DFP intoxication induces PAI-1 expression but not colocalization in CD68 positive cells. **b** PAI-1 and IBA1 colocalization geometric mean ration (GMR) with 95% CI in DFP (n=10-12) versus VEH (n=10-12) animals. There was no difference in the colocalization effect by time point nor region, so estimates of group differences were averaged across time points and regions. Acute DFP intoxication induces PAI-1 expression but not colocalization in microglia. In panels **a** and **b**, CIs in blue indicate significant results (p<0.05). A GMR with a 95% CI that crosses the 1.0 intercept indicates no significant difference between groups. A GMR with a 95% CI above or below the 1.0 intercept indicates a significant increase or decrease, respectively.
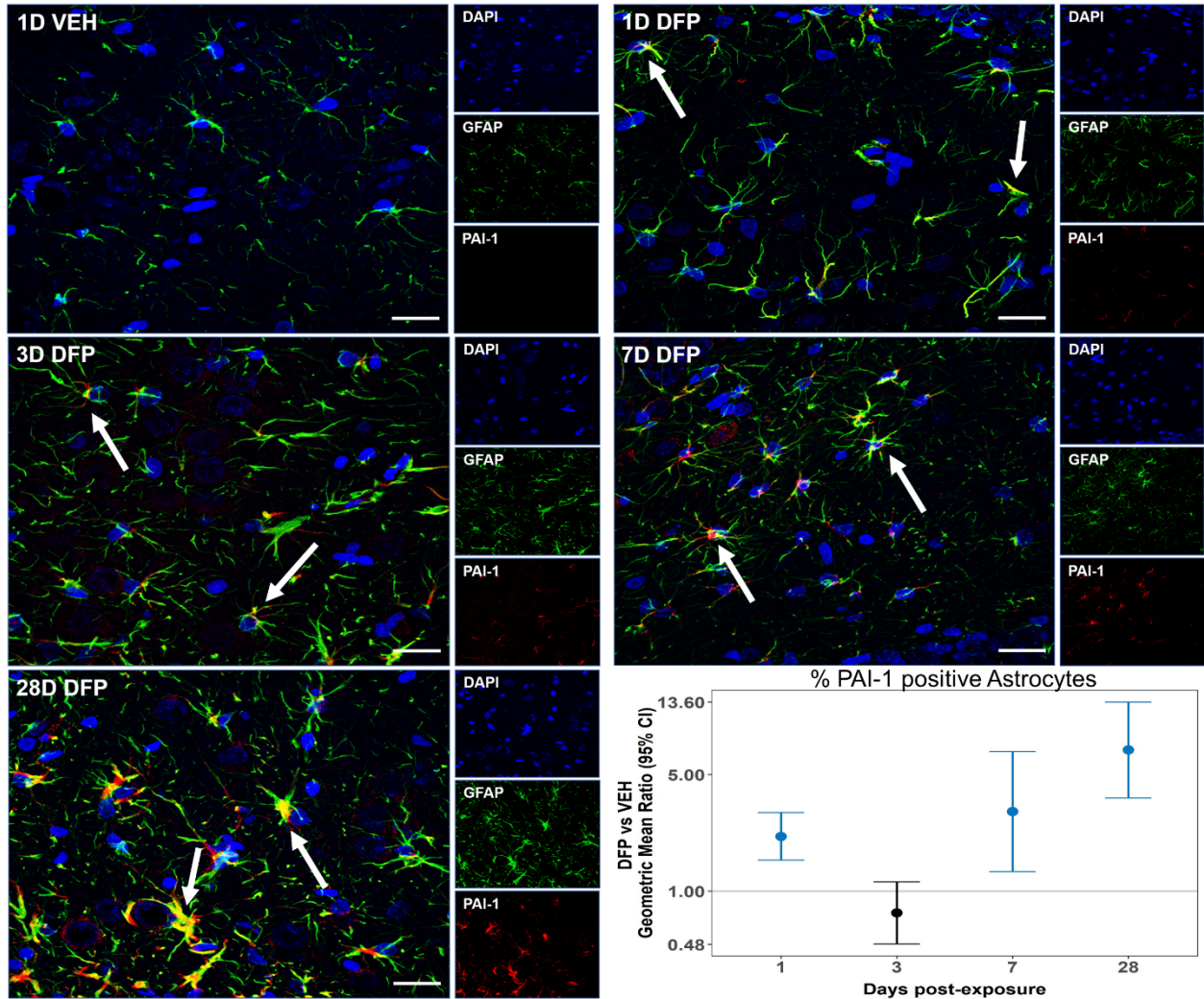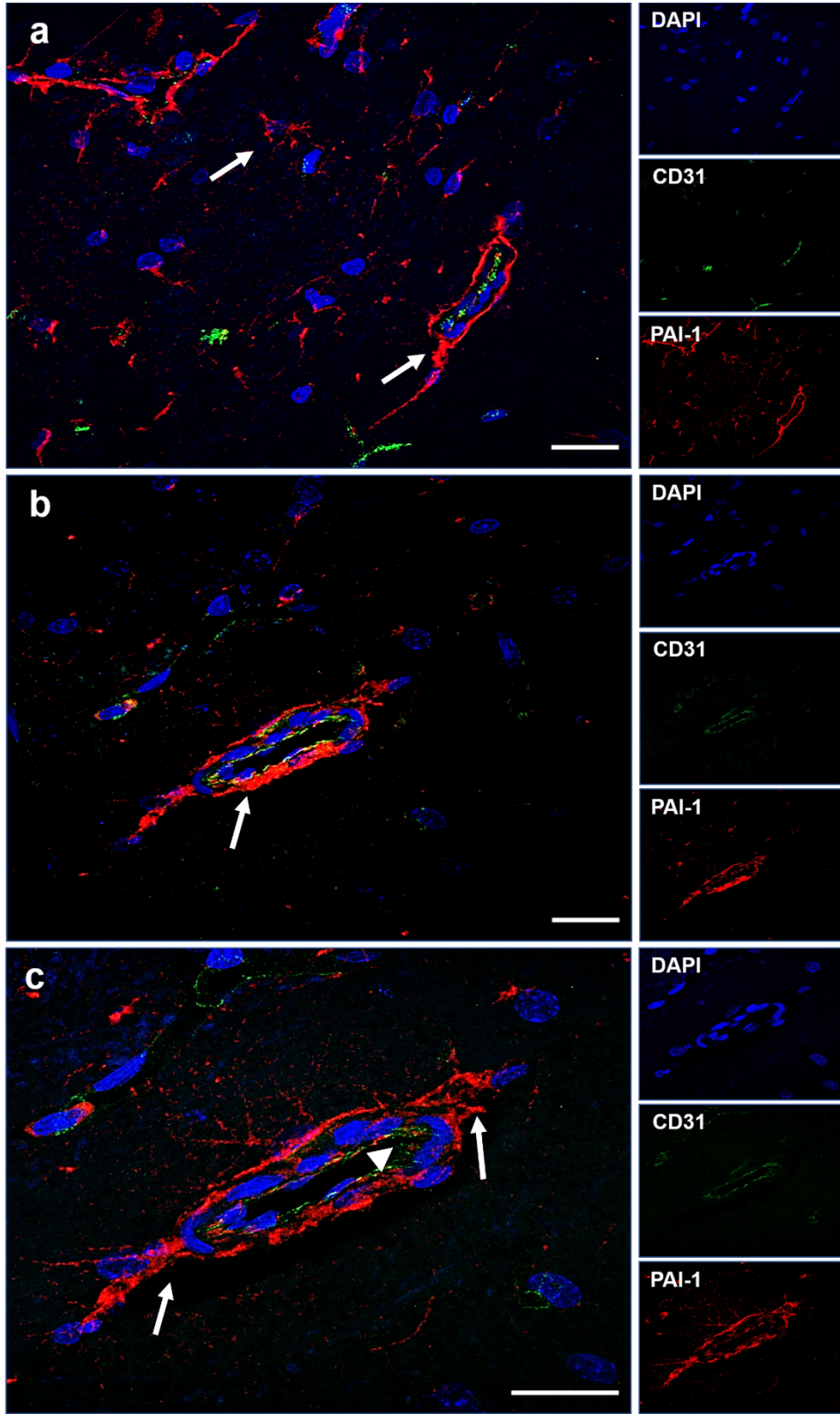
Fig. 10 Acute DFP intoxication induces PAI-1 expression in astrocytic subpopulations over 28 days post-exposure. Representative photomicrographs of a VEH animal compared to DFP animals with PAI-1 (red) and GFAP (green) immunoreactivity in the hilus of the hippocampus at 1, 3, 7 and 28 days post-exposure. Sections were counterstained with DAPI to identify cell nuclei. Bar = 20 μm. Arrows indicate PAI-1 immunoreactivity in astrocytic cell bodies and processes persisting out to 28 days post-exposure. Regional PAI-1 and GFAP colocalization geometric mean ratio (GMR) with 95% CI in DFP (n=10-12) versus VEH (n=10-12) animals. DFP animals had a significantly higher percentage of astrocytes expressing PAI-1 than VEH in all brain regions at 1, 7, and 28, but not 3 days post-exposure. There was no difference in the colocalization effect by region, so estimates of group differences were averaged across regions. A GMR with a 95% CI that crosses the 1.0 intercept indicates no significant difference

between groups. A GMR with a blue 95% CI above or below the 1.0 intercept indicates a significant increase or

decrease (p<0.05), respectively

Fig. 11 Acute DFP intoxication induces PAI-1 expression in distal astrocytic processes adjacent to endothelial cells at 1 day post-exposure **a-b** Representative photomicrographs of PAI-1 (red) and CD31 (green) immunoreactivity in the hippocampus of a DFP-intoxicated animal at 1 day post-exposure. Sections were counterstained with DAPI to identify cell nuclei. Arrows indicate PAI-1 immunoreactivity in glial cell bodies and processes surrounding blood vessels with minor colocalization of PAI-1/CD31. Bar = 20 µm. **c** A higher magnification image of panel b. Bar =20 µm. Arrow indicates PAI-1 immunoreactivity in glial cell bodies and processes surrounding blood vessels and possible endothelial cells with minor colocalization of PAI-1/CD31. Arrowhead indicates higher amounts of CD31 positive immunoreactivity within the vessel and little CD31 immunoreactivity on the outer edge of the vessel where the majority of PAI-1 immunoreactivity occurs

7. Supplementary Methods

7.1 Western blotting

Supernatants of homogenized brain samples prepared as described in section 2.3 were used in western blot assay to validate PAI-1 antibodies. Briefly, samples were boiled with 4x Laemmli buffer (Bio-Rad Laboratories, Hercules, CA, USA) with freshly added 10% ß-mercaptoethanol (Sigma Aldrich) for 5 min. Fifty ng of standard PAI-1 protein (Molecular Innovations, Novi, MI, USA) as the positive control and 10 µg of brain supernatants were loaded into wells of a Bolt^{TM} 10% Bis-Tris Mini Protein Gel (Invitrogen, Thermo Fisher Scientific, USA) for SDS-PAGE. Proteins were then transferred to PVDF membrane (Invitrogen) by iBlot 2 Dry Blotting System (Invitrogen) following the manufacturer's instructions. Membranes were blocked using Odyssey Blocking Buffer (#927-40000, Licor, USA) with 0.1% Tween-20 (Thermo Fisher Scientific) for 1 h and then incubated with rabbit anti-human PAI-1 primary antibody (Table 2) in blocking buffer overnight at 4 ˚C. Subsequently, after three washes with 1x PBST buffer, membranes were incubated with IRDye 680RD goat anti-rabbit secondary antibody (Table 3) at room temperature for 1 h. Images were acquired on an Odyssey® CLx Imaging System (Licor) and analyzed using ImageJ 1.51m9(http://imagej.nih.gov/ij/; NIH).

7.2 Quantification of biomarker expression

ImageXpress Micro XLS High Content Analysis System custom module step by step guide for each co-stain (https://ucdavis.box.com/s/7txi692shr2epdnuhm1gzcju9t8j1sns).

7.2.1 PAI/NeuN: % of neurons expressing PAI-1

1. Find round objects was used to identify DAPI positive nuclei.

2. Find blobs was used to identify NeuN positive neurons.

3. Logical operations were used to identify DAPI positive neurons.

4. Keep marked objects was used to keep the overall shape of the neurons from step 2 but only include neurons that also had DAPI signal.

5. Simple threshold was used to filter out positive PAI-1 signal from background. Positive signal was defined as signal at least twice the intensity of background. In most cases positive signal was at least 3 times higher than background.

6. Grow objects without touching was used on the DAPI positive nuclei to slightly increase their size since PAI-1 could colocalize right outside of the nucleus and usually is found on the cell surface or within the cytoplasm.

7. Logical operations were used to filter out DAPI positive cells that did not express PAI-1.

8. Keep marked objects was used to keep count of the neurons that also had an overlap with PAI-1 positive signal.

9. Measure mask was used to analyze the proportion of NeuN positive neurons that had PAI-1 positive signal.

7.2.2 PAI/IBA1 and PAI/CD68: % of microglia and phagocytic microglia expressing PAI-1

1. Find round objects was used to identify DAPI positive nuclei.

2. Find blobs was used to identify CD68 positive cells.

3. Logical operations were used to identify DAPI positive and CD68 positive cells. This is used for the colocalization analysis for the percentage of CD68 positive cells that are co-expressing PAI-1.

4. Keep marked objects uses the cells from step 3 and the shapes from step 1 to allow for the entire cell to be marked as CD68 positive.

5. Find round objects was used to identify IBA1 positive cell bodies and some intersecting processes.

6. Find fibers was used to retain microglial processes and mark non-fibrous objects which were the microglial cell bodies.

7. Logical operations were used to retain the entire microglial cell.

8. Keep marked objects was used to keep the overall shape of the microglia, but only include microglia that also had DAPI signal.

9. A filter mask was applied to microglia to individualize each cell so that overlapping cells were limited. For example, without the filter mask, two or more overlapping microglia or microglia that have "connecting" processes would only be counted as one total cell. The filter mask allows us to remove this problem while still allowing the cells to have processes.

10. Simple threshold was used to filter out positive PAI-1 signal from background. Positive signal was defined as signal at least twice the intensity of background. In most cases positive signal was at least 3 times higher than background.

11. Logical operations were used to filter out DAPI positive cells that did not express PAI-1.

12. Logical operations were used to identify IBA1 positive microglia that also expressed PAI-1.

13. Keep marked objects was used to keep the count of microglia that also had an overlap with PAI-1 positive signal.

14. Logical operations were used to identify CD68 positive cells that also expressed PAI-1.

15. Keep marked objects was used to keep the count of CD68 positive cells that also had an overlap with PAI-1 positive signal.

16. Measure mask was used to analyze the proportion of IBA1 positive microglia that had PAI-1 positive signal. It was simultaneously used to analyze the proportion of CD68 positive cells that had PAI-1 positive signal.

7.2.3 PAI/GFAP: % of astrocytes expressing PAI-

1. Find round objects was used to identify DAPI positive nuclei.

2. Find round objects was used to identify GFAP positive cell bodies and some intersecting processes.

3. Logical operations were used to identify DAPI positive astrocytes.

4. Find fibers was used to retain astrocyte processes and mark non-fibrous objects which were the astrocytic cell bodies.

5. Logical operations were used again to retain the entire astrocyte cell.

6. A filter mask was applied to astrocytes to individualize each cell so that overlapping cells were limited. For example, without the filter mask, two or more overlapping astrocytes or astrocytes that have "connecting" processes would only be counted as one total cell. The filter mask allows us to remove this problem while still allowing the cells to have processes.

7. Logical operations were used to include full astrocytes with processes and other astrocytes that did not have processes in the plane but had their cell body in view.

8. Simple threshold was used to filter out positive PAI-1 signal from background. Positive signal was defined as signal at least twice the intensity of background. In most cases positive signal was at least 3 times higher than background.

9. Grow objects without touching was used on the DAPI positive nuclei to slightly increase their size since PAI-1 could colocalize right outside of the nucleus and usually is found on the cell surface or within the cytoplasm.

10. Logical operations were used to filter out DAPI positive cells that did not express PAI-1.

11. Logical operations were used to identify GFAP positive astrocytes that also expressed PAI-1.

12. Measure mask was used to analyze the proportion of GFAP positive astrocytes that had PAI-1 positive signal.

8. Supplementary Data:
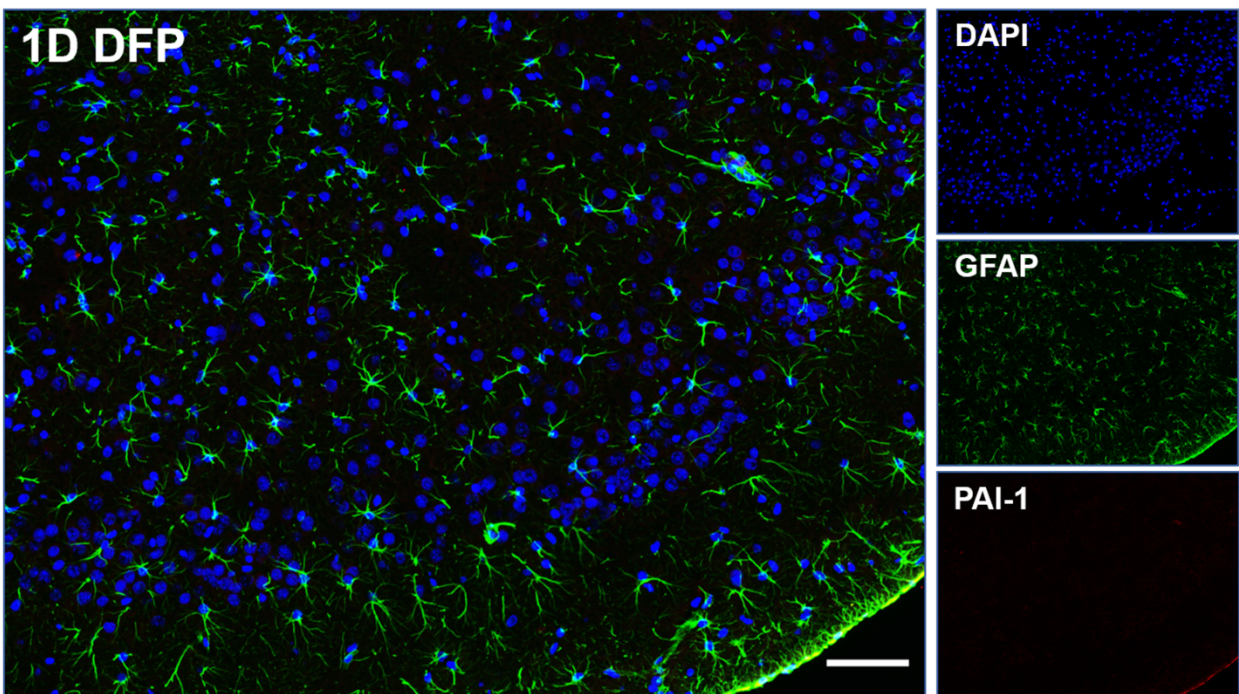
Fig. S1 DFP-induced PAI-1 expression is largely excluded from the piriform cortex at 1 day post-exposure. Representative photomicrographs of a DFP animal with PAI-1 (red) and GFAP (green) immunoreactivity. Sections were counterstained with DAPI to identify cell nuclei. Bar represents 80 μm
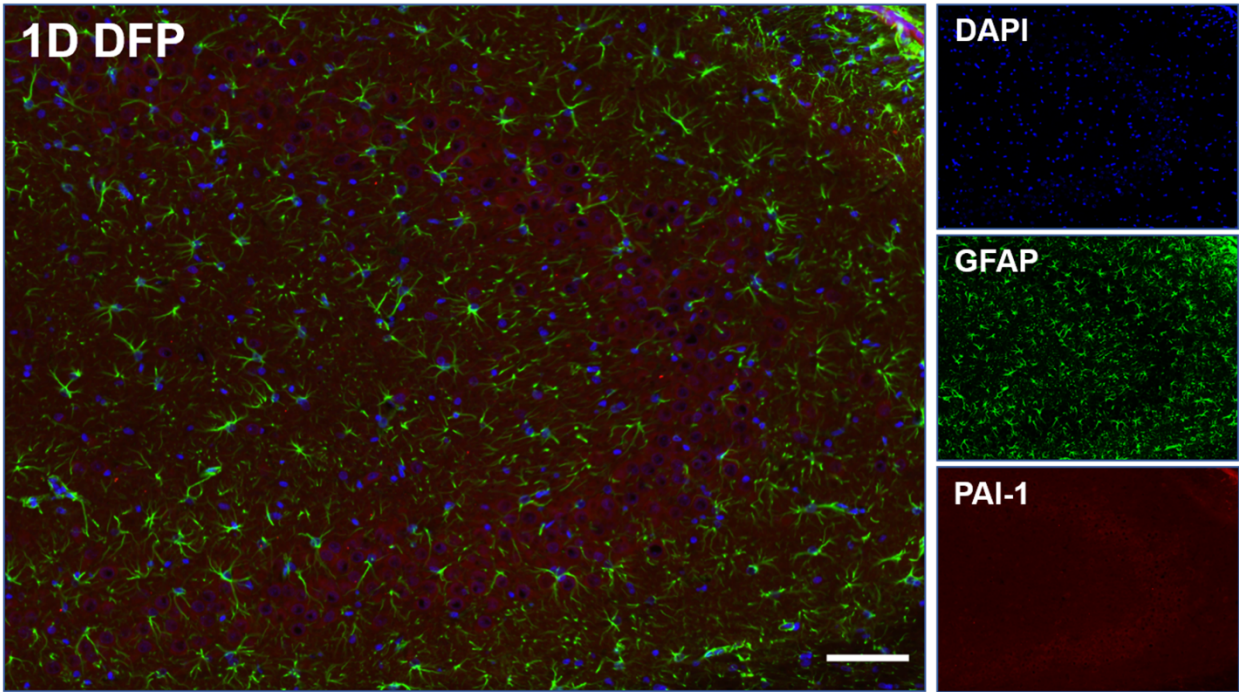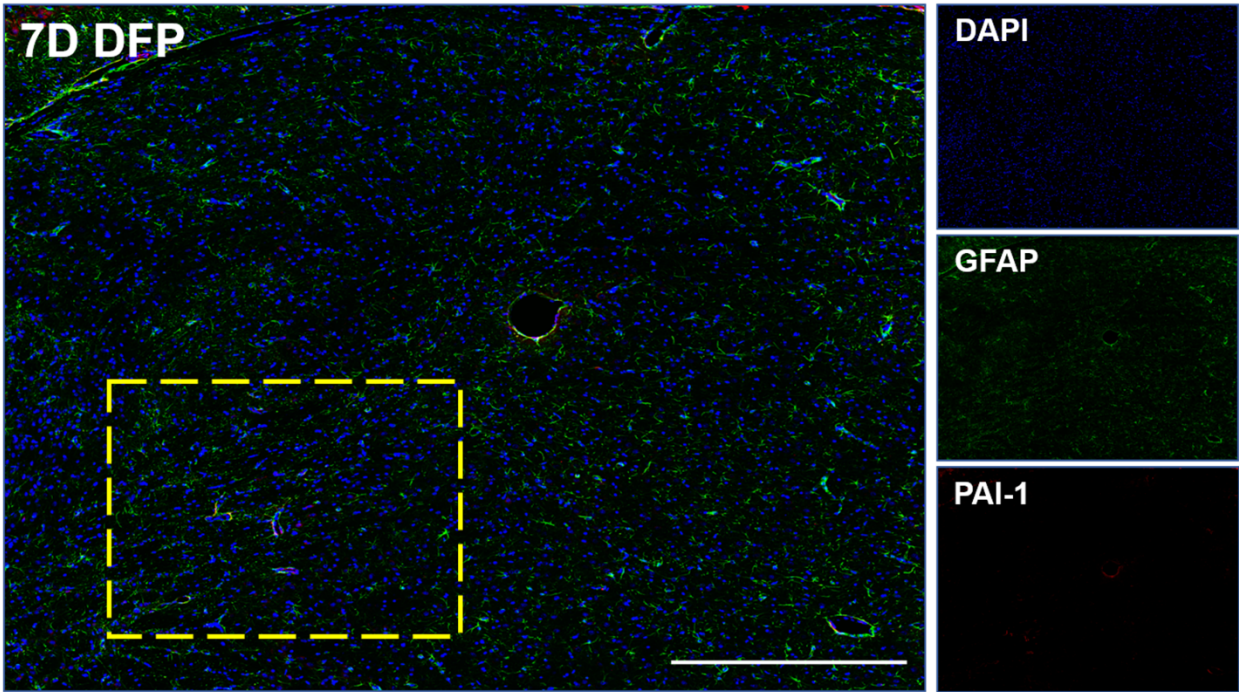
Fig. S2 DFP-induced PAI-1 expression is largely excluded from the CA3 region of the hippocampus at 1 day post-exposure. Representative photomicrographs of a DFP animal with PAI-1 (red) and GFAP (green) immunoreactivity. Sections were counterstained with DAPI to identify cell nuclei. Bar represents 80 μm

Fig.S3 DFP-induced PAI-1 expression is minimal in the thalamus at 7 days post-exposure. Representative photomicrographs of a DFP animal with PAI-1 (red) and GFAP (green) immunoreactivity. PAI-1 immunoreactivity is not observed in the majority of astrocytes but is apparent around blood vessels. A higher magnification image of the region within the yellow box is shown in **Fig S4**. Sections were counterstained with DAPI to identify cell nuclei. Bar represents 500 μm
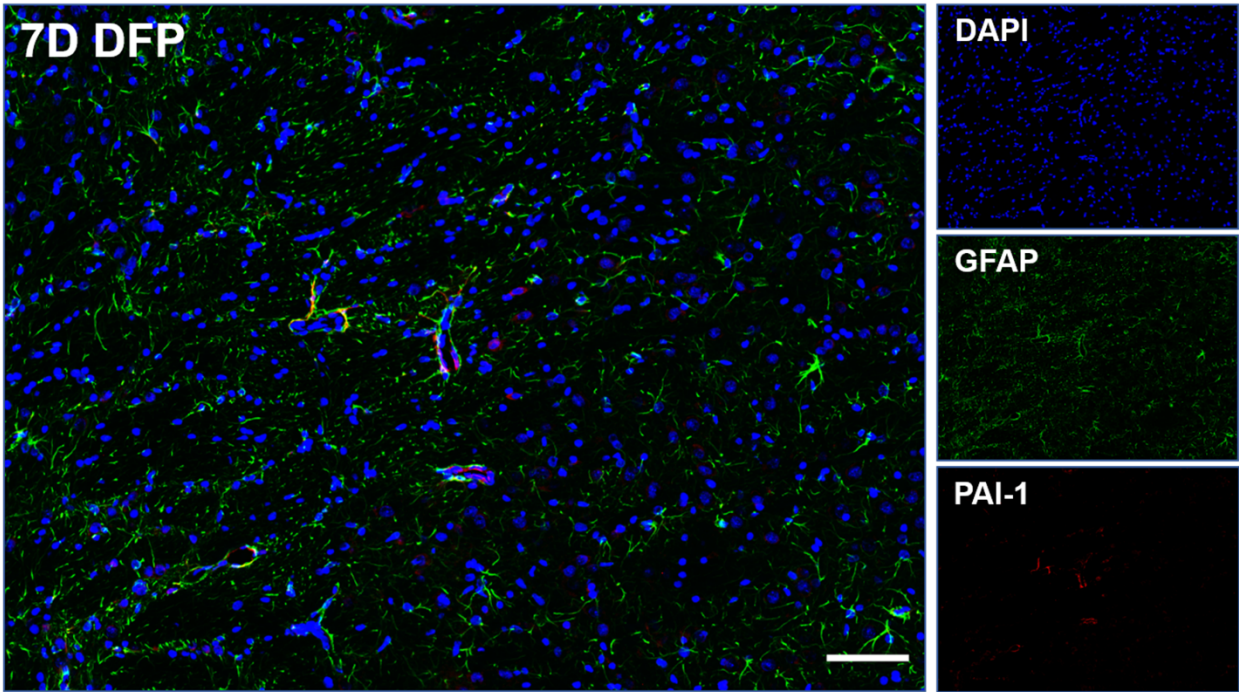
Fig. S4 DFP-induced PAI-1 expression is minimal and largely excluded from the thalamus at 7 days post-exposure. Higher magnification photomicrograph of **Fig. S3** of a DFP animal with PAI-1 (red) and GFAP (green) immunoreactivity. PAI-1 immunoreactivity is not observed in the majority of astrocytes but is observed around blood vessels. Sections were counterstained with DAPI to identify cell nuclei. Bar represents 80 µm

9. Supplementary Controls

Western Blot

MyBioSource:
rabbit anti-human PAI-1
polyclonal
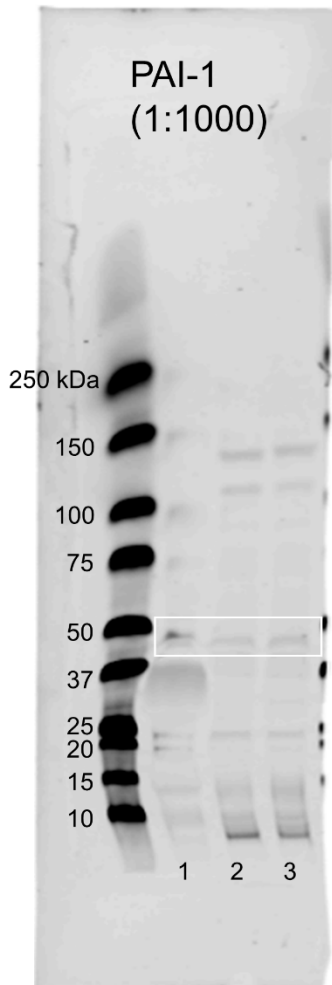
PAI-1
(1:1000)

1: PAI-1 standard (ELISA kit) – 0.05 ng
2: 1d DFP – 20 ug
3: VEH – 20 ug

250 kDa
150
100
75
50
37
25
20
15
10

1   2   3

Fig. S5 Validation of MyBioSource polyclonal antibody against PAI-1 standard from the Molecular Innovations total PAI-1 ELISA kit. Corresponding band slightly below 50 kDa on lane 1 demonstrates specificity of MyBioSource PAI-1 antibody. No dark bands appear above 50 kDa demonstrating highly specific binding to pure PAI-1 protein. Lanes 2 and 3 are brain extracts from DFP and VEH rats. High molecular weight bands likely

correspond to PAI-1 complexes with tPA [13] . Low molecular weight bands likely correspond to PAI-1 reactive

center cleavage [32].

a

WB result from Abcam for PAI-1
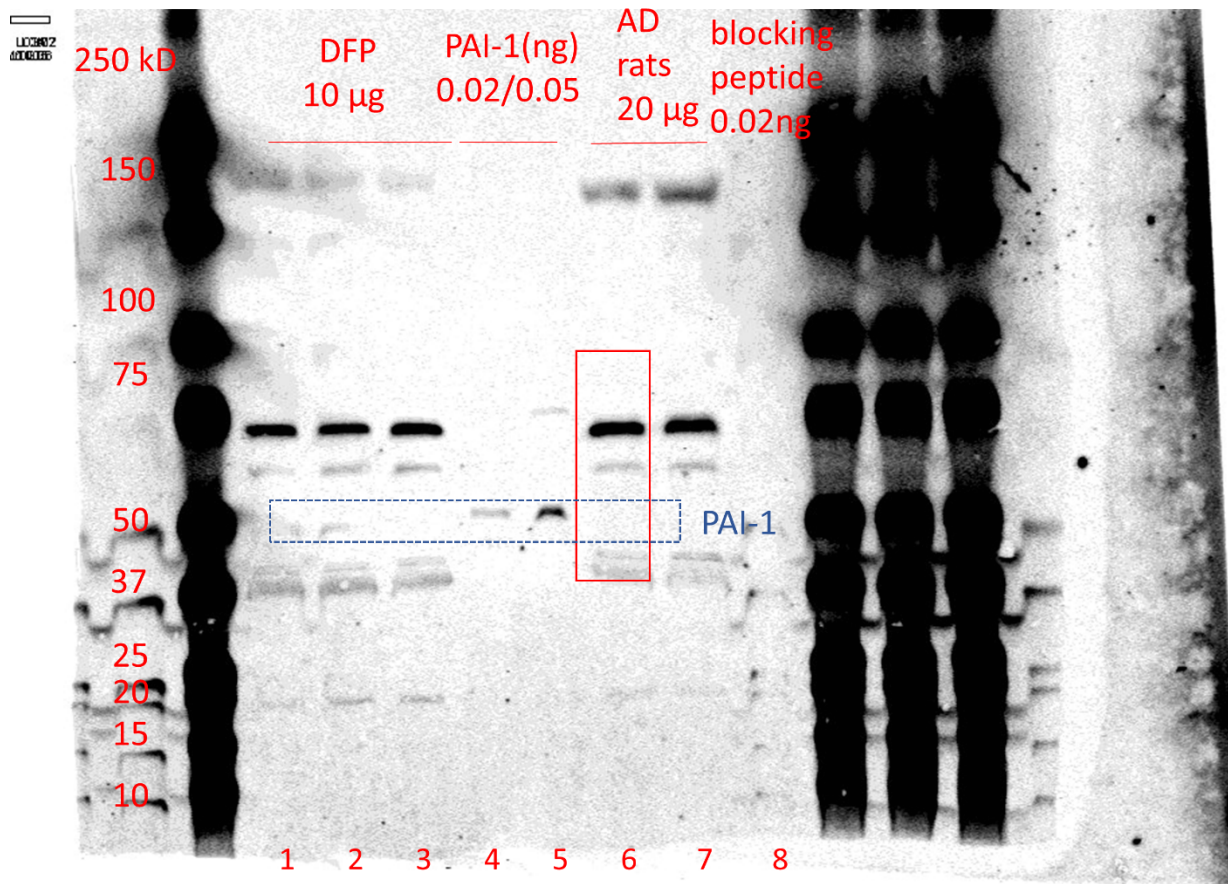in human endothelial cell lysate

Abcam 66705

b

DFP
10 µg

PAI-1(ng)
0.02/0.05

AD
rats
20 µg

blocking
peptide
0.02ng

PAI-1

1 2 3 4 5 6 7 8
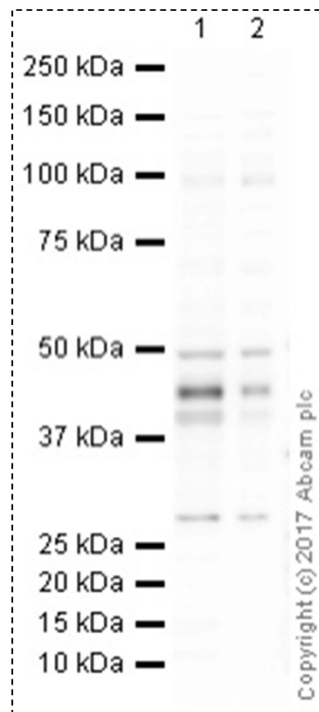
Fig. S6 a Image taken from Abcam website demonstrating PAI-1 Polyclonal antibody validity in human endothelial cell line. **b** Validation of Abcam polyclonal antibody against DFP rat brain lysates, transgenic Alzheimer's Disease rat brain lysates, and PAI-1 standard used in Molecular Innovations total PAI-1 ELISA kit. Lanes 1-3 correspond to 10 ug of DFP rat brain lysates. Lanes 4-5 correspond to 0.02 and 0.05 ng, respectively, of purified PAI-1 standard from Molecular Innovations total PAI-1 ELISA kit. Lanes 6-7 correspond to 20 ug of transgenic Alzheimer's Disease rat brain lysates. Lane 8 corresponds to purified protein, 0.02 ng, incubated with PAI-1 blocking peptide. Lanes 4-5 demonstrate specificity of Abcam polyclonal antibody to a purified PAI-1 protein but other lanes (1-3, 6-7) demonstrated non-specific binding to an unknown protein around 65 kDa invalidating the antibody. Even with the example WB provided by Abcam in human endothelial cell lysate (**a**), there are multiple bands below and around 45 kDa, with a faint band around 100 kDa
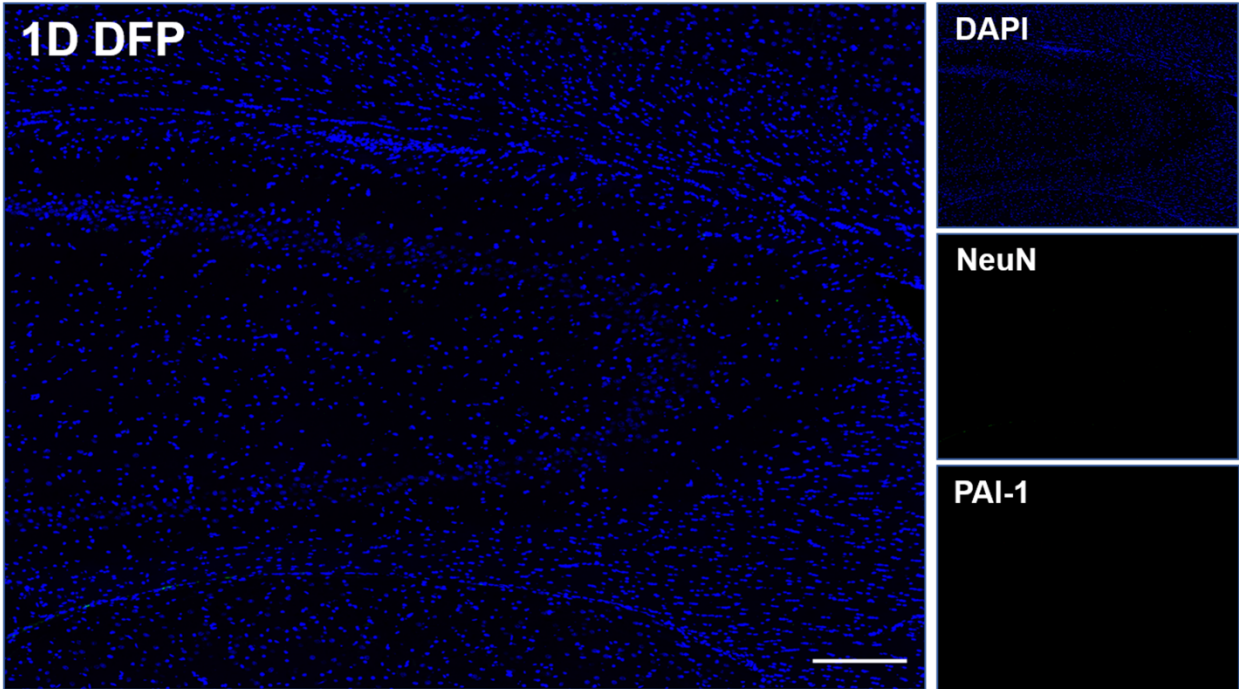
Fig. S7 NeuN and PAI-1 secondary only control demonstrates no positive immunoreactivity. Representative photomicrograph of a DFP animal with PAI-1 (red) and NeuN (green) immunoreactivity. PAI-1 and NeuN immunoreactivity is not observed due to the absence of primary antibody. Secondary antibody shows no specific staining patterns. Sections were counterstained with DAPI to identify cell nuclei. Bar represents 200 μm
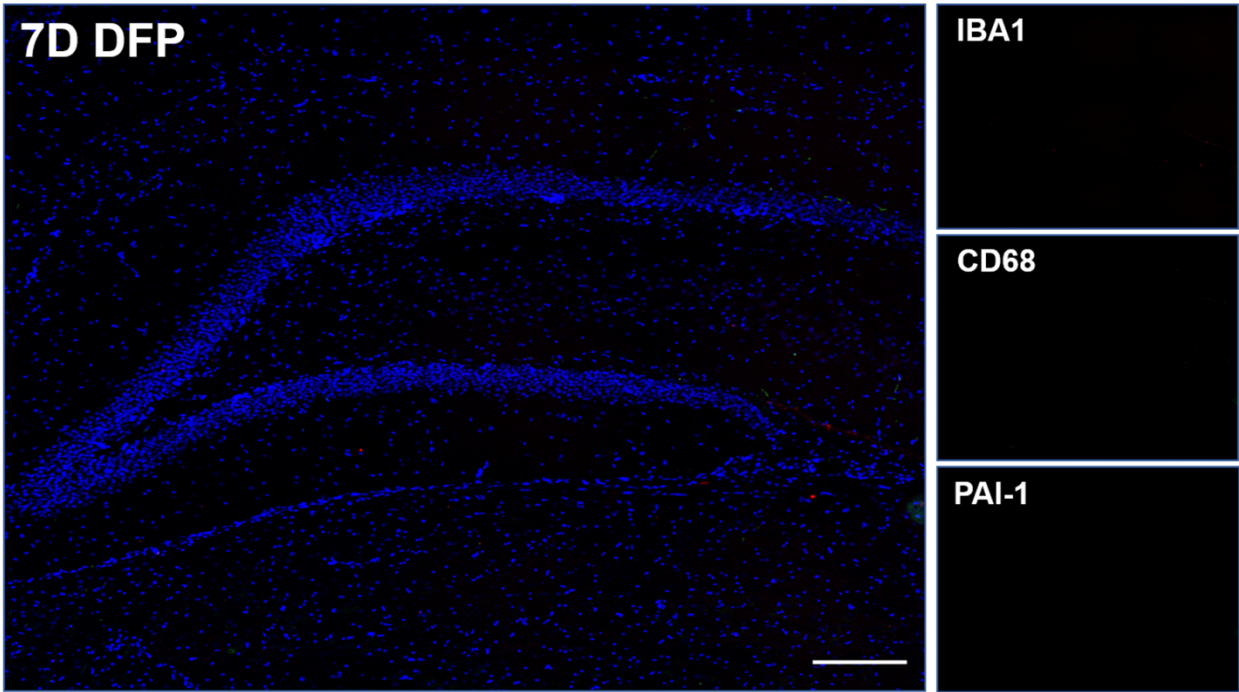
Fig. S8 IBA1, CD68, and PAI-1 secondary only control demonstrates no positive immunoreactivity.
Representative photomicrograph of a DFP animal with IBA1 (red), CD68 (green), and PAI-1 (cyan)
immunoreactivity. IBA1, CD68, and PAI-1 immunoreactivity is not observed due to the absence of primary
antibody. Secondary antibody shows no specific staining patterns. Sections were counterstained with DAPI to
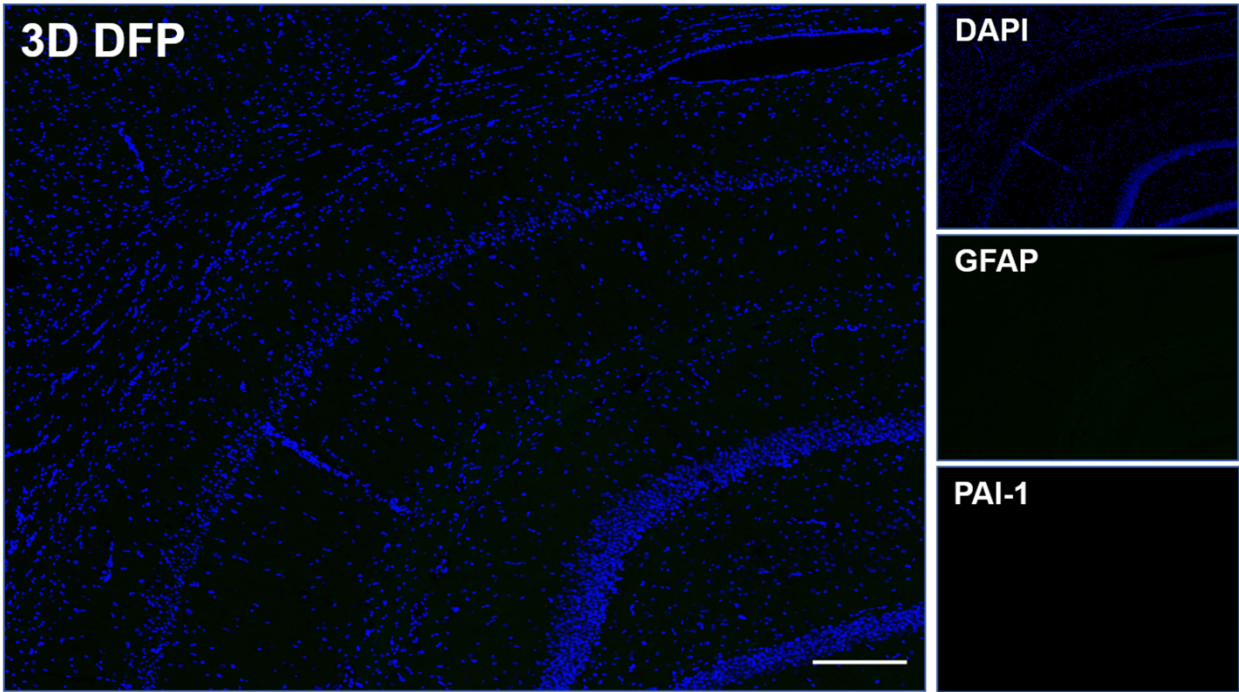identify cell nuclei. Bar represents 200 μm

Fig. S9 GFAP and PAI-1 secondary only control demonstrates no positive immunoreactivity. Representative photomicrograph of a DFP animal with PAI-1 (red) and GFAP (green) immunoreactivity. PAI-1 and GFAP immunoreactivity is not observed due to the absence of primary antibody. Secondary antibody shows no specific staining patterns. Sections were counterstained with DAPI to identify cell nuclei. Bar represents 200 μm
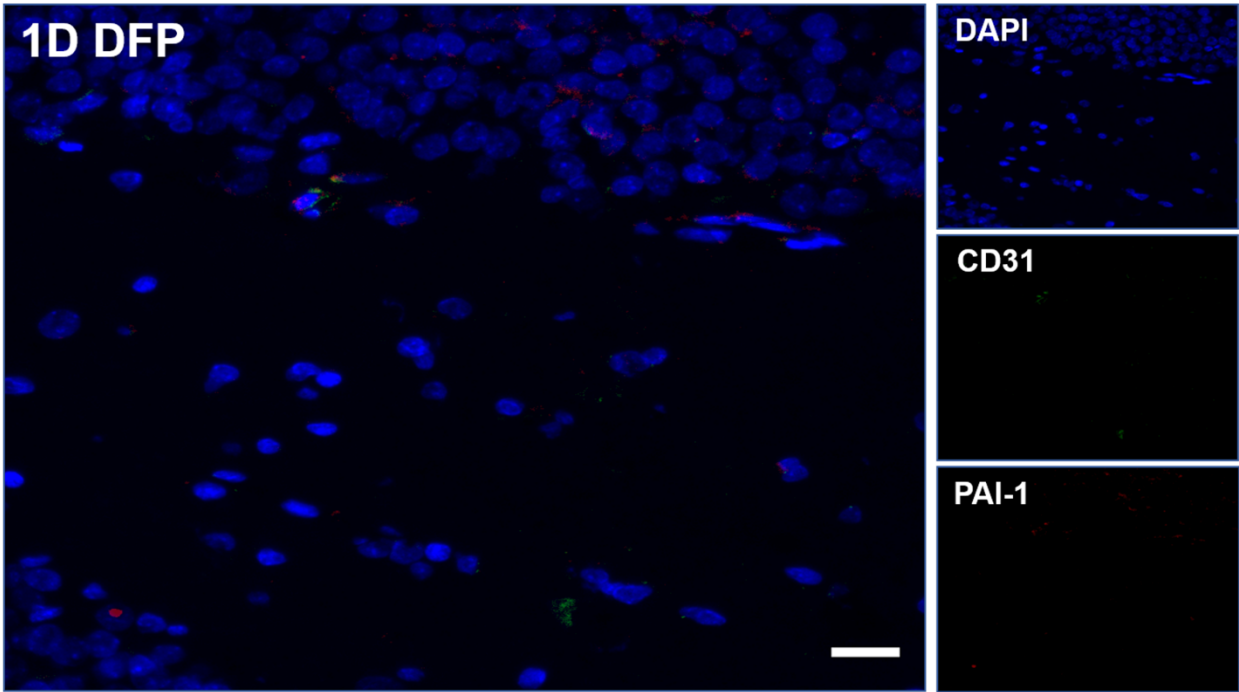
Fig. S10 CD31 and PAI-1 secondary only control demonstrates no positive immunoreactivity. Representative photomicrograph of a DFP animal with PAI-1 (red) and CD31 (green) immunoreactivity. PAI-1 and CD31 immunoreactivity is not observed due to the absence of primary antibody. Secondary antibody shows no specific staining patterns. Sections were counterstained with DAPI to identify cell nuclei. Bar represents 20 μm